Hindawi
International Journal of Chemical Engineering
Volume 2024, Article ID 6690487, 24 pages
https://doi.org/10.1155/2024/6690487

Research Article

Numerical Study on Heat Transfer and Release Characteristics of Key Components in Electrically Heated Tobacco Products

Bo Zhang[1], **Lingjun Xiao**[2], **Jiejie Huang**[2], **Zhiguo Wang**[1], **Naiping Gao**[2], **Wen Du**[1], **Bo Kong**[1], **Zhiwei Sun**[1], **Ping Huang**[1], **Jianxin Ren**[1], **Bin Li**[3] and **Yihan Gao**[4]

[1]*Technology Center, China Tobacco Hunan Industrial Co., Ltd, Changsha 410007, China*
[2]*School of Mechanical Engineering, Tongji University, Shanghai 201804, China*
[3]*Zhengzhou Tobacco Research Institute of CNTC, Zhengzhou 45000, China*
[4]*Shanghai New Tobacco Product Research Institute Co., Ltd, Shanghai 200000, China*

Correspondence should be addressed to Lingjun Xiao; xiaolingjun@tongji.edu.cn and Zhiguo Wang; 3687248842@qq.com

Received 21 August 2023; Revised 4 March 2024; Accepted 23 March 2024; Published 15 April 2024

Academic Editor: Nicole Vorhauer-Huget

Electrically heated tobacco products (EHTPs) could release effective aerosol components from tobacco materials at relatively low temperatures without a burning phenomenon. It is essential to grasp the temperature distribution and release mechanism of key components in heated tobacco materials. The existing experimental studies have provided initial insights into the thermodynamic behavior of tobacco materials under various conditions. However, current numerical models are still in their early stages of development, with the majority failing to correlate heat transfer with component release. Based on this, a coupled numerical model of gas flow, heat transfer, and the release of key components in the electrically heated tobacco product is established in this study, which exhibits improvements in revealing the internal heat and mass transfer characteristics in the porous media of tobacco and is capable of evaluating the influence of component contents and product design parameters. The release rates of water, glycerol, and nicotine components are quantitatively described by the first-order Arrhenius formula, and the transport of heat and gas flow is simulated using the Navier-Stokes equation. The accuracy of the model is validated through experiments, including temperature monitoring at multiple measurement points and determination of residual contents in the tobacco substrate after each puff. The simulation results suggest that an appropriate component ratio and tobacco filler mass can enhance both the release amount and release efficiency of key components, and reducing either the diameter or length of the tobacco section can help to improve the heat transfer performance. A slower heating rate matched with longer preheating times enables the complementary release of water and glycerol components, which helps to regulate the uniformity of component content in the aerosol to some extent. This study helps to provide suggestions for the design and optimization of electrically heated tobacco products.

1. Introduction

With the increasing awareness of the health risks associated with smoking, new tobacco products are being marketed as less toxic alternatives to traditional cigarettes in order to lower emissions of toxicants and reduce harm [1, 2]. Among them, the electrically heated tobacco product is a new type of tobacco product emerging rapidly in the tobacco industry in recent years [3], accounting for 42.7% of the global market share of new tobacco products in 2021. An electric heating sheet or heating needle is typically used to heat the tobacco substrate to temperatures sufficient to release water and volatile organic compounds such as nicotine, without initiating a self-sustaining smoldering combustion process [4]. As the heating temperature (below 500°C, mostly 350°C) is lower than the combustion temperature of traditional cigarettes (600°C–900°C), it can effectively reduce the harmful components produced by pyrolysis and thermal synthesis of tobacco at high temperatures [5, 6].

Generally, the electrically heated tobacco product is composed of a tobacco section, a hollow section, and a filter section [7, 8]. Different types of wrapping paper are used to securely bond and affix each individual section. Among them, the tobacco section is the core area that determines the quality of the product. The heat and mass transfer characteristics in the tobacco section are directly related to its internal temperature distribution and the release process of key components. Various factors, such as the initial component ratio in the tobacco substrate, the tobacco filler mass, and the temperature profile of the heater, will significantly affect the taste of the aerosol. There are studies on the pyrolysis process and release characteristics of water, glycerol, and nicotine in tobacco materials under the condition of a fixed heating temperature or continuous heating processes. It is found that at low temperatures, free water and some loosely bound water are first released. As heat is gradually transferred into the tobacco substrate, the temperature continues to rise, leading to the subsequent release of nicotine and glycerol. Glycerol undergoes minimal pyrolysis during heating, with the majority transferring to the gas phase at temperatures between 150°C and 250°C [9]. Nicotine is transferred into the gas phase by vaporization, and the release rate reaches its peak value in the range of 160~200°C [10]. Water, glycerol, and nicotine account for more than 80% of the aerosol mass [11–13]. At temperatures exceeding 200°C, other low-molecular-weight gases (such as CO, CO_2, and ammonia), aldehydes, ketones, and other primary pyrolysis products are released [14], and all these gas-phase components form and aggregate in the pores of porous tobacco media. Zheng et al. [15] test the aerosol components and the release characteristics of the aerosol former, nicotine, and other substances at 11 equidistant temperature points in the range of 200~470°C. The results reveal that within the temperature range of 260°C to 320°C, the glycerol content in the aerosol increased significantly as the heating temperature rose. Gómez-Siurana et al. [16] find that only water and CO_2 are released from tobacco materials under 150°C through real-time data of the Fourier transform infrared spectrum. In addition, a series of investigations have been conducted to explore the thermophysical properties of tobacco [17–19] and the reaction kinetic mechanism of volatile release [20–24], which contribute to a better understanding of the heat and mass transfer processes inside the electrically heated tobacco products.

For the design of a suitable component ratio in the tobacco substrate and the temperature profile of the heating element, it often costs a lot to adopt experimental means for parameter adjustments. With the rapid advancement of computer technology, numerical simulation methods have been extensively used to study the law of heat and mass transfer [25, 26]. The tobacco section of the electrically heated tobacco product is mainly filled with cut tobacco or tobacco sheets, which can be considered as porous media characterized by a tobacco substrate and void space. Based on the theory of porous media, several studies [27–29] have established foundational heat transfer models for the tobacco section of the electrically heated tobacco product, which are capable of predicting the temperature distribution within the gas-phase domain under static heating conditions and during dynamic puffing, but do not take the release of components into consideration. Nordlund and Kuczaj [30] establish a relatively complete mathematical model for the entire electrically heated tobacco product, which includes the heat and mass transfer processes of gas-phase components in anisotropic porous media, as well as the transient volume and mass changes in multicomponent aerosols, but the changes in thermal properties and density of the tobacco substrate during heating are not considered. Wang et al. [31] experimentally derive the relationship between the volume-averaged temperature of the tobacco section and the release of key components, employing a simplified lumped parameter method, which treats the electrically heated tobacco product as a single point. However, as the model assumes a uniform distribution of temperature and key component concentrations throughout the tobacco section, it fails to provide a three-dimensional temperature distribution and detailed insight into the heat transfer process within the tobacco section. Current numerical models are still in the early stages of development.

To sum up, existing experimental results have provided valuable insights into the thermodynamic behavior of tobacco materials under various conditions; however, they have not yet been able to yield sufficient guidance for practical applications. However, most numerical simulations fail to correlate heat transfer with component release. Therefore, based on the existing models' foundation, a coupled numerical model of gas flow, heat transfer, and the release of key components in the electrically heated tobacco product is established in this study, which exhibits improvements primarily in the following aspects: firstly, it helps reveal the internal heat and mass transfer characteristics in the porous media of tobacco; secondly, it accounts for changes in the thermal properties of tobacco and the permeability of filamentous porous media during the heating process; and lastly, the accuracy of the model is validated through experiments, including temperature monitoring at multiple measurement points and determination of residual contents in the tobacco substrate after each puff, which allows for a better match with actual conditions. The effects of the initial component ratio, the tobacco filler mass, the dimensions of the tobacco section, and the temperature profile of the heater on temperature distribution and the release characteristics of key components within the tobacco section are investigated under dynamic puffing conditions. The commercial software Fluent is used to solve the coupled model through user-defined functions (UDFs). The results are helpful in further understanding the release mechanisms of water, glycerol, and nicotine and can provide suggestions for the design and optimization of electrically heated tobacco products.

2. Numerical Modelling

2.1. Physical Model. The electrically heated tobacco product studied in this paper is mainly composed of a tobacco section, a hollow section, and a filter section. The diameter of the EHTP is 7.8 mm, and the length of the tobacco section is 13.5 mm. The diameter of the heating needle is 2.15 mm, the head is conical, and its length is 2 mm. The total depth of insertion is 13.8 mm. In the numerical simulation, the heat

transfer process, component release through phase transition, and chemical reactions in the tobacco section are mainly focused. Therefore, the influence of ventilation holes can be ignored. A two-dimensional axisymmetric model, as shown in Figure 1, is established to reach a faster calculation speed.

In the numerical simulation, the following assumptions are adopted to simplify the solution:

(1) As the stacking of tobacco shreds is characterized by randomness and disorder, it is technically hard to obtain their anisotropic thermal properties. Therefore, based on the macroscopic solution method in the field of porous media, the tobacco substrate in the EHTP is considered as a uniform porous medium with uniform thermal properties in all directions.

(2) As only a small fraction of tobacco near the heater surface undergoes mild pyrolysis reactions during heating, the impact of tobacco pyrolysis on heat transfer is considered minimal in the tobacco substrate. Additionally, the thermal expansion of the tobacco substrate is typically negligible within the temperature range of the heating process. Therefore, it can be assumed that the density of the tobacco substrate does not change during heating.

(3) The heat transfer process and component release caused by temperature rise in the tobacco section are mainly focused, ignoring the detailed evolution including the condensation and interception of gas-phase components in the hollow section and the filter section.

(4) Based on ideal heating conditions, the potential local temperature differences on the surface of the heater are neglected. Besides, compared to thermal conduction, the contribution of thermal radiation to heat transfer is considered to be relatively minor and can be ignored.

It is important to highlight that assumption (1), which treats the tobacco substrate in the EHTP as uniform and isotropic porous media rather than considering its actual anisotropic thermal properties, could potentially result in errors in heat transfer and thereby affect the temperature distribution within the tobacco section. However, it is worth noting that mathematical models based on the assumption of isotropic porous media have been shown to yield satisfactory results [27–29]. The close match between numerical and experimental results indicates that when the most relevant physical and chemical processes are considered in the numerical model, the predictive errors of the model are maintained within an acceptable range. However, although the actual stacking pattern of tobacco shreds may exhibit anisotropic characteristics, it is reasonable to treat the tobacco substrate as isotropic on a macroscopic scale due to the random distribution of tobacco shreds. This perspective is particularly applicable when focusing on the overall heating effect rather than specific local details, which aligns with the focus of this study.

2.2. Governing Equations. During the operation of the electrically heated tobacco product, the gas and solid phases cannot reach the thermal equilibrium state within the short duration of each puff. Therefore, with the assumption of a local thermal imbalance between phases, a solid zone that is spatially coincident with the porous fluid zone is defined. In this case, the conservation equations for energy are solved separately for the fluid and solid zones, and each variable is treated as intrinsic to its respective domain [32]. The governing equations of the mathematical model are as follows.

The energy equation for the gas phase is as follows:

$$\frac{\partial}{\partial t}\left(\phi\rho_g E_g\right) + \nabla\cdot\left(\vec{v}\left(\rho_g E_{\mathrm{g}} + p\right)\right) = \nabla\cdot\left(\phi k_{\mathrm{g}}\nabla T_{\mathrm{g}} - \left(\sum_i h_i J_i\right) + \left(\tau\cdot\vec{v}\right)\right) + S_g^h + h_{\mathrm{gs}}A_{\mathrm{gs}}\left(T_{\mathrm{s}} - T_{\mathrm{g}}\right). \tag{1}$$

The energy equation for the solid phase is as follows:

$$\frac{\partial}{\partial t}\left((1-\phi)\rho_s E_s\right) = \nabla\cdot\left((1-\phi)k_s\nabla T_s\right) + S_s^h + h_{gs}A_{gs}\left(T_g - T_s\right), \tag{2}$$

where t is time, s; ϕ is the porosity of porous media; ρ_g is the gas-phase density, kg/m^3; ρ_s is the solid-phase density, kg/m^3; E_{g} is the total gas-phase energy, J/kg; E_s is the total solid-phase energy, J/kg; v is the gas-phase velocity, m/s; p is the local pressure, Pa; k_{g} is the gas-phase thermal conductivity, W/(m·K); k_s is the solid-phase thermal conductivity, W/(m·K); h_i is the enthalpy of gas-phase component i, J/kg; J_i is the diffusion flux of gas-phase component i, Kg/(m^3·s); τ is the stress tensor, Pa; S_g^h is the gas-phase enthalpy source term, S_s^h is the solid-phase enthalpy source term, W/m^3; $S_s^h = \sum_k(-\Delta H_k)(\partial\rho_k/\partial t)$, W/m^3; h_{gs} is the heat transfer coefficient for the fluid/solid interface, W/(m^2·K); A_{gs} is the interfacial area density, m^{-1}; T_{g} is the gas-phase temperature, K; and T_s is the solid-phase temperature, K.

The momentum equation for the gas phase is as follows:

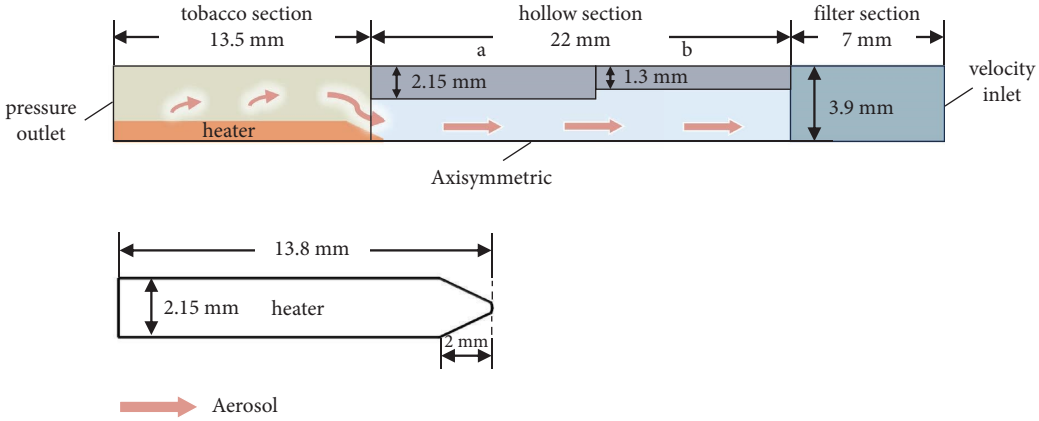

Figure 1: Schematic diagram of the two-dimensional axisymmetric model of the electrically heated tobacco product.

$$\frac{\partial\left(\phi\rho_g\vec{v}\right)}{\partial t}+\nabla\cdot\left(\phi\rho_g\vec{v}\vec{v}\right)=-\phi\nabla p+\nabla\cdot(\phi\tau)+\phi\vec{B_f}+\phi S_i, \tag{3}$$

where B_f is the body force, N/m^3; S_i is the source term of porous media, $S_i=-(\mu/\alpha\vec{v}+C_2 1/2\rho_g|\vec{v}|\vec{v})$, where μ is the dynamic viscosity of the gas phase, kg/(m·s); α is the permeability of porous media, m^2; and C_2 is the inertial resistance factor.

The component transport equation is as follows:

$$\frac{\partial\left(\phi\rho_g Y_i\right)}{\partial t}+\nabla\cdot\left(\rho_g\vec{v}Y_i\right)=\nabla\cdot\left(\rho_g D_i\phi\nabla Y_i\right)+\phi S_{\rho_i}^{s\longrightarrow g}, \tag{4}$$

where Y_i is the mass fraction of component i in the gas phase, $Y_i=\rho_i/\rho_g$, ρ_i is the density of component i in the gas phase, kg/m^3; and D_i is the diffusion coefficient of component i in the gas phase, m^2/s, which is computed by the Chapman–Enskog formula using kinetic theory [33].

The mass conservation equation is as follows:

$$\frac{\partial\left(\phi\rho_g\right)}{\partial t}+\nabla\cdot\left(\rho_g\vec{v}\right)=\phi S_\rho^{s\longrightarrow g}, \tag{5}$$

where $S_\rho^{s\longrightarrow g}$ is the mass transfer source term of gas-solid two phases, which can be obtained by accumulating the amount of component i released at each moment:

$$S_\rho^{s\longrightarrow g}=\sum_{i=1}^{n}S_{\rho_i}^{s\longrightarrow g}=\sum_{i=1}^{n}m_s\frac{dS_{Y_i}^{s\longrightarrow g}}{Vdt}, \tag{6}$$

where m_s is the tobacco filler mass, kg; $S_{Y_i}^{s\longrightarrow g}$ is the mass of component i released per unit mass of tobacco at each moment, mg/mg; and V is the volume of the entire domain of the tobacco section, m^3.

According to the combustion reaction of traditional cigarettes [34, 35], the release rates of the three key components of water, glycerol, and nicotine in our model are calculated by the Arrhenius kinetic parameters. To standardize integral expressions, all release processes are quantitatively described by the first-order Arrhenius formula. The activation energy and pre-exponential factors can be obtained by fitting the thermogravimetric curve of tobacco substrates [20] (see Section 3.1 for the values of the kinetic parameters).

$$\frac{dS_{Y_i}^{s\longrightarrow g}}{dt}=k_i\left(S_{Y_i}^{*}-S_{Y_i}^{s\longrightarrow g}\right),$$
$$k_i=A_i e^{\left(-E_i/RT_s\right)}, \tag{7}$$

where k_i is the chemical reaction rate, 1/s; $S_{Y_i}^{*}$ is the maximum mass of component i that can be released under infinite time and high pyrolysis intensity, mg/mg; A_i is the pre-exponential factor, 1/s; E_i is the chemical reaction activation energy, kJ/mol; and R is the universal gas constant, 8.314 J/(mol·K).

2.3. Boundary and Initial Conditions. The boundary and initial conditions in the simulation, along with their associated parameters, are listed in Table 1. At the outlet of the filter section, the Health Canada Intense (HCI) puffing protocol (55 mL, 2 s sinusoidal puffs every 30 s) for 8 puffs is specified, and the first puff starts at 15 s after heating. For mass fraction boundary conditions, the release rates of the three key components within the tobacco domain are calculated by the Arrhenius kinetic parameters and are loaded into governing equations as a source term by the user-defined functions (UDFs). Zero diffusive flux is specified for species boundary conditions at the walls. The operating pressure is set at a constant value of 101325 Pa.

2.4. Numerical Method. The mixed aerosol emitted from the electrically heated tobacco product includes air, water, glycerol, and nicotine, as well as other constituents. The compressibility effects of air, water, glycerol, and nicotine components, as well as the gas mixtures, are treated by employing the ideal gas law. The specific heat capacity of air, water, glycerol, and nicotine components adopts a polynomial function of temperature, with the properties of air obtained from Zhang et al. [36] and properties of water, glycerol, and nicotine components referenced from Data Handbook of Chemistry and Chemical Engineering [37] and the CAMEO Chemicals database [38]. The thermal

Table 1: Overview of boundary and initial conditions in the simulation.

Boundary and initial conditions		Conditions settings	Parameters
Boundary conditions	Inlet	Outlet of the filter section: velocity inlet with the velocity set according to the HCI puffing protocol	v, p in equations (1), (3)–(5)
	Outlet	Inlet of the tobacco section: pressure outlet with the gauge pressure set to 0	
	Wall	Surface of the heating element: time-varying temperature based on experimentally measured data, as shown in Figure 2 Top and bottom of the heating element: heat flux = 0 W/m^2 Outer walls: convective heat transfer boundary condition with heat transfer coefficient = 65.25 W/(m^2·K) and ambient fluid temperature = 300 K All walls: nonslip conditions	E_g, T_g, E_s, and T_s in equations (1) and (2)
	Tobacco domain	Enthalpy source terms and mass transfer source terms loaded by the UDFs	S_g^h, S_s^h, and $S_\rho^{s\longrightarrow g}$ in equations (1), (2), and (5)
Initial conditions	All domains	Initial temperature = 26.85°C Initial velocity = 0	T_g and T_s in equations (1) and (2) v in equations (1), (3), (4), and (5)
	Fluid domain	Initial pressure = 101325 Pa Mass fraction of air = 1	p in equations (1) and (3)
	Tobacco domain	Water content = 11.38 wt%; Glycerol content = 16.48 wt%; Nicotine content = 1.13 wt%	Y_i and $S_{\rho_i}^{s\longrightarrow g}$ in equations (4) and (5)

Note. "wt%" stands for "weight percent."

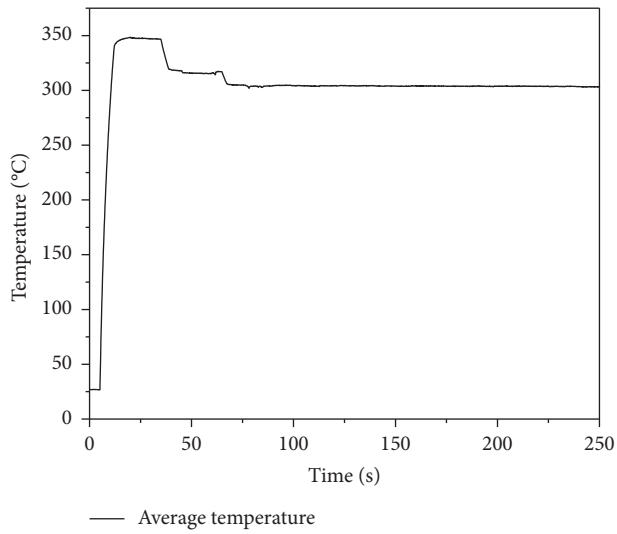

Figure 2: Time-varying temperature of the heating element surface.

conductivity and viscosity of each component are calculated according to the kinetic theory [39], which is updated and dependent on temperature. The initial values of these properties for the simulation are listed in Table 2. Other parameters, including the density, initial porosity, and permeability of tobacco, as well as the equivalent diameter of tobacco shreds, are obtained through experimental measurements. Meanwhile, changes in the thermophysical properties of the tobacco accumulation body under different component contents and heating temperatures are considered in this study (see Appendix for details).

The numerical simulations are performed with ANSYS Fluent 19.0 software. The source terms are loaded into governing equations by the user-defined functions (UDFs). The governing equations are discretized by the finite volume method and linearized and solved by the implicit mode. The second-order upwind scheme is used for the discretization of all terms. The pressure-velocity coupling is implemented through the SIMPLEC algorithm. The second-order implicit time integration scheme is employed in terms of time discretization. The time step is set to 0.05 s, and the convergence criteria of globally scaled residuals are set to 10^{-3} for all variables. The Courant number remains below 1 throughout the simulation, which ensures the stability of the numerical solution.

2.5. Grid Independence Analysis. To evaluate the grid independence of the computational domain, six different grid schemes (9963, 16324, 23982, 41681, 57589, and 99486) are tested. A hybrid mesh setup, incorporating both triangular and quadrilateral elements, is utilized for discretization. The temperatures of three monitoring lines in the tobacco section at the maximum flow rate of the last puff are selected for comparison. It can be seen from Figure 3 that the temperatures of the models with 9963 and 41681 grids differ significantly from those of other models, and there is no further improvement in calculation accuracy when the number of grids exceeds 57589. The puff-by-puff release amounts of the three key components including water, glycerol, and nicotine are shown in Figure 4. It can be observed that different grid schemes result in some variations in the release amounts of components, but the maximum discrepancy is less than 3.29%. Based on the predictive performance of different grid schemes on both temperatures and release amounts of the three key components, the model with grid number 57589 is selected to discretize the computational domain in this study.

3. Experiment and Validation

3.1. Experimental Determination of Chemical Composition of Tobacco. Before puffing, the determination of the initial contents of water, glycerol, and nicotine in the tobacco substrate is conducted using gas chromatography according to CORESTA recommended method no. 57 [40], no. 60 [41], and no. 62 [42], respectively. The water content is determined by extraction in a methanol solution containing isopropanol as an internal standard, followed by gas chromatographic (GC) analysis with thermal conductivity detection (TCD). The glycerol is determined by extraction in a methanol solution containing 1,3-butanediol as an internal standard, followed by gas chromatographic (GC) analysis with flame ionization detection (FID). The nicotine content is determined by liquid/liquid extraction into an organic solvent containing an internal standard, followed by gas chromatographic (GC) analysis with flame ionization detection (FID). To ensure an adequate amount of the target components for the analytical indicators of water, glycerol, and nicotine, five EHTP sticks (with wrapping paper) are placed together in a 50 mL centrifuge tube. Their mass is measured and recorded, followed by the addition of the appropriate volume of extraction solvent, and then, the mixture is agitated in preparation for gas chromatographic analysis. Three parallel experiments are conducted for each component, and the results are reported as weight percent (wt%). Accordingly, the initial contents are determined as 11.38 wt% for water, 16.48 wt% for glycerol, and 1.13 wt% for nicotine in the tobacco substrate.

Table 2: Parameters used in the simulation.

Parameter	Value
Tobacco density (kg/m^3)	919.9
Tobacco particle density (kg/m^3)	1040
Initial porosity of tobacco	0.420
Initial permeability of tobacco (m^2)	3.41×10^{-10}
Equivalent diameter of tobacco shreds (mm)	0.39
Thermal conductivity of water vapor (W/(m·K))	0.0261
Specific heat capacity of water vapor (J/(kg·K))	2014
Water vapor viscosity (kg/(m·s))	1.34×10^{-5}
Thermal conductivity of glycerol vapor (W/(m·K))	0.0205
Specific heat capacity of glycerol vapor (J/(kg·K))	1916
Glycerol vapor viscosity (kg/(m·s))	9.87×10^{-6}
Thermal conductivity of nicotine vapor (W/(m·K))	0.0212
Specific heat capacity of nicotine vapor (J/(kg·K))	1813
Nicotine vapor viscosity (kg/(m·s))	9.35×10^{-6}
Enthalpy of water evaporation (J/kg)	2.26×10^6
Enthalpy of glycerol evaporation (J/kg)	6.64×10^5
Heat transfer coefficient of the outer wall of tobacco section (W/(m^2·K))	65.25

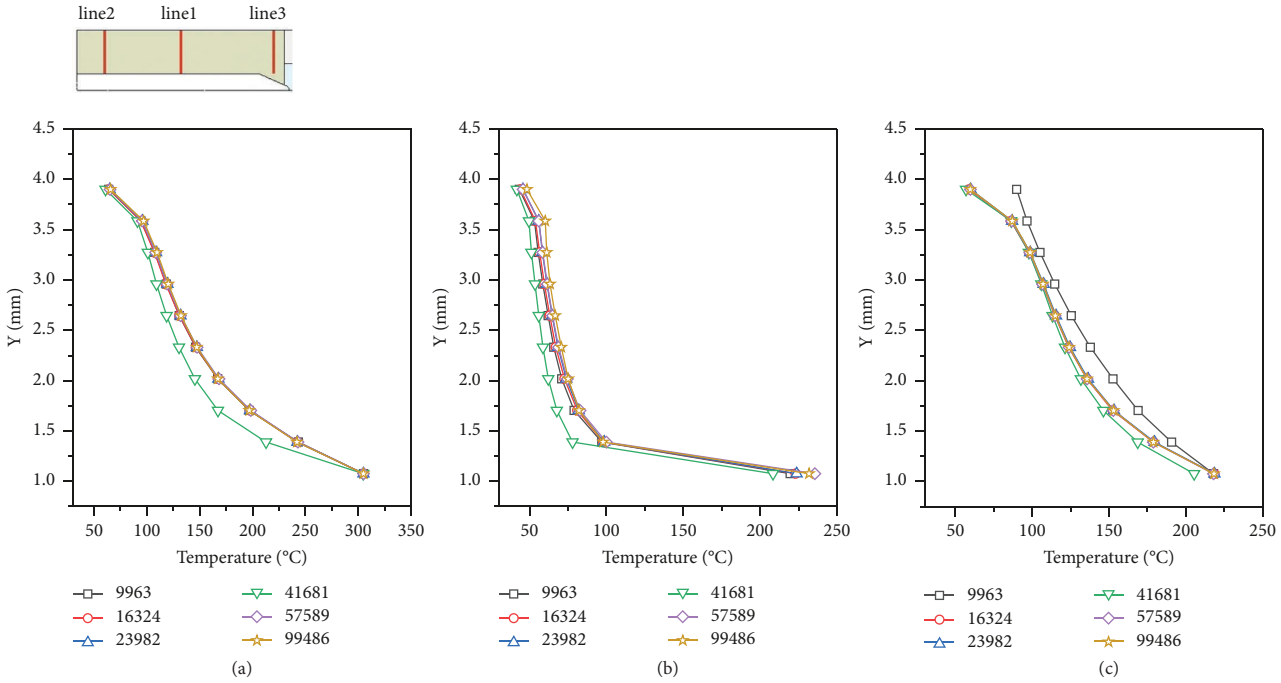

Figure 3: Comparison between the temperatures of (a) line 1, (b) line 2, and (c) line 3 at the maximum flow rate of the last puff ($t = 226$ s) with different grid numbers.

3.2. Pyrolysis Experiment in a Tube Furnace. Based on the combustion reaction of traditional cigarettes [34, 35], the release rates of water, glycerol, and nicotine components in our model are quantitatively calculated using the Arrhenius formula. To unify the integral expressions, all release processes are simplified to first-order reactions. To obtain the release characteristics of water, glycerol, and nicotine in the tobacco substrate under different temperature conditions, a tobacco pyrolysis experiment is carried out in a tube furnace to calibrate the reaction kinetic parameters for the tobacco substrate in the studied EHTP. Five identical EHTP samples, each filled with 200 mg of tobacco, are used in the experiment. Fifteen puffs are taken according to the HCI puffing protocol (55 mL, 2 s sinusoidal puffs every 30 s). The release amounts of the three key components are measured at seven equidistant temperature points from 50°C to 350°C.

According to the pyrolysis experimental results (pyrolysis temperature: 50~350°C; pyrolysis time: 1 minute; analysis temperature: 250°C; analysis time: 5 minutes), water is continuously released during the heating process, exhibiting two release peaks below 160°C and another release peak above 225°C, which can be approximately divided into three release

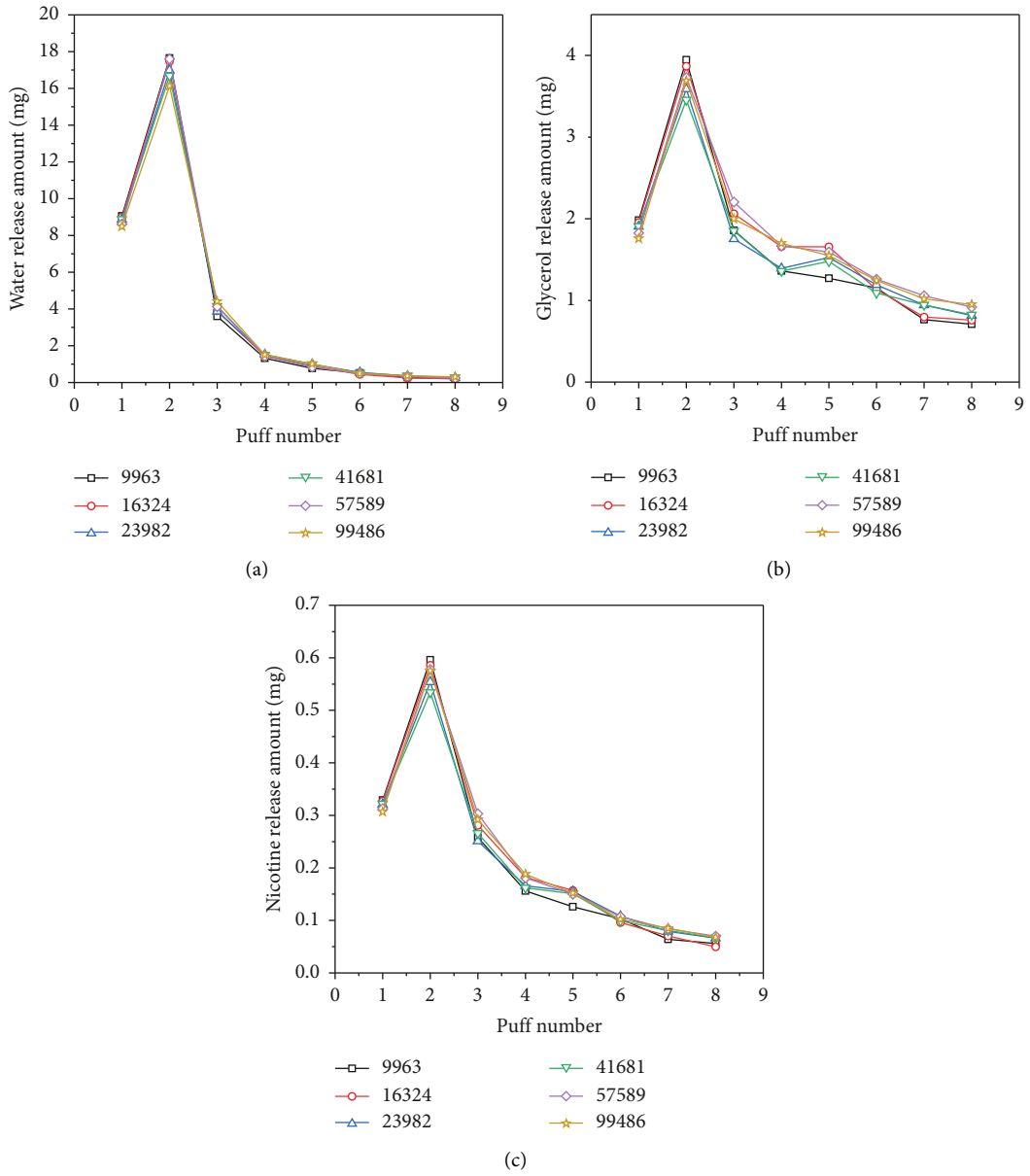

Figure 4: Puff-by-puff release amounts of (a) water, (b) glycerol, and (c) nicotine with different grid numbers.

processes. Correspondingly, for glycerol and nicotine, a primary phase transition occurs at temperatures above 100°C, accompanied by a secondary phase transition over a broad temperature range, which can be approximately divided into two release processes. The reaction kinetic parameters for the tobacco substrate in the studied EHTP are then calibrated and fitted to obtain the release rates of water, glycerol, and nicotine that could closely match the experimental curves, as shown in Figure 5. Results of the fitted reaction kinetic parameters for the tobacco substrate in the studied EHTP are listed in Table 3.

3.3. Validation

3.3.1. Validation of the Temperature. Due to the limited geometric dimensions of the electrically heated tobacco product, it is impractical to directly measure the internal temperature within the tobacco section of the product. In this regard, a self-designed and constructed scale-up experimental device is developed. The schematic diagram and detailed geometric parameters of the device are presented in Figure 6 and Table 4, respectively.

The experiment is conducted under room temperature conditions at 27°C. The experimental device regulates the flow rate by adjusting the glass rotor flow meter (k) connected to the external vacuum pump (l), thus simulating the puffing process of electrically heated tobacco products. A DC-regulated power supply (j) provides electrical energy (at an applied voltage of 50 V) to the heater (d). A paperless recorder (a) equipped with the K-type armored microfine thermocouple (b) is utilized to collect real-time temperature data, including the surface temperature of the heater at measurement point ①, the internal temperatures at measurement points ②~⑤ within the

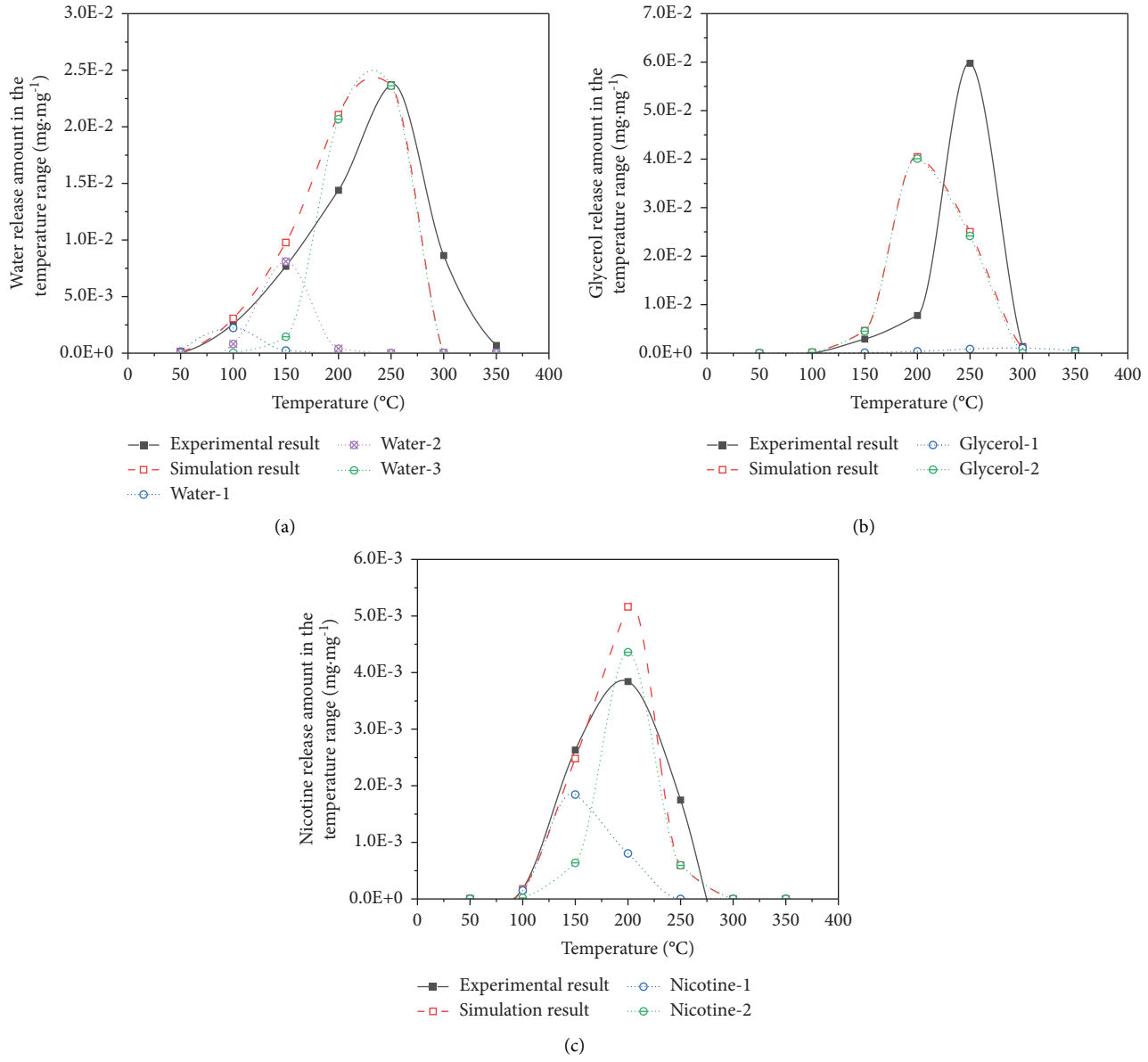

Figure 5: Comparison of the experimental results with the calculated results under different temperature conditions: (a) water release results at a single point temperature; (b) glycerol release results at a single point temperature; (c) nicotine release results at a single point temperature.

Table 3: Results of the fitted reaction kinetic parameters for the studied tobacco substrate.

Component	Pre-exponential factor A (1/s)	Activation energy E (kJ/mol)	Order n (–)	Maximum release rate (mg/mg)
Water 1	3.03×10^8	76.8	1	0.0950
Water 2	2.01×10^9	92.8	1	0.0154
Water 3	1.61×10^8	100.0	1	0.0020
Glycerol 1	1.27×10^2	49.8	1	0.0750
Glycerol 2	1.96×10^7	89.9	1	0.0878
Nicotine 1	3.19×10^7	81.5	1	0.0048
Nicotine 2	2.19×10^8	96.4	1	0.0065

Note. (1) "Water 1" denotes the first phase transition that promotes the release of water, and "Water 2" denotes the secondary phase transition. The naming principle for other numbered reactions is the same; (2) the maximum release rate = the maximum mass of component that can be released during the release process/the total mass of tobacco.

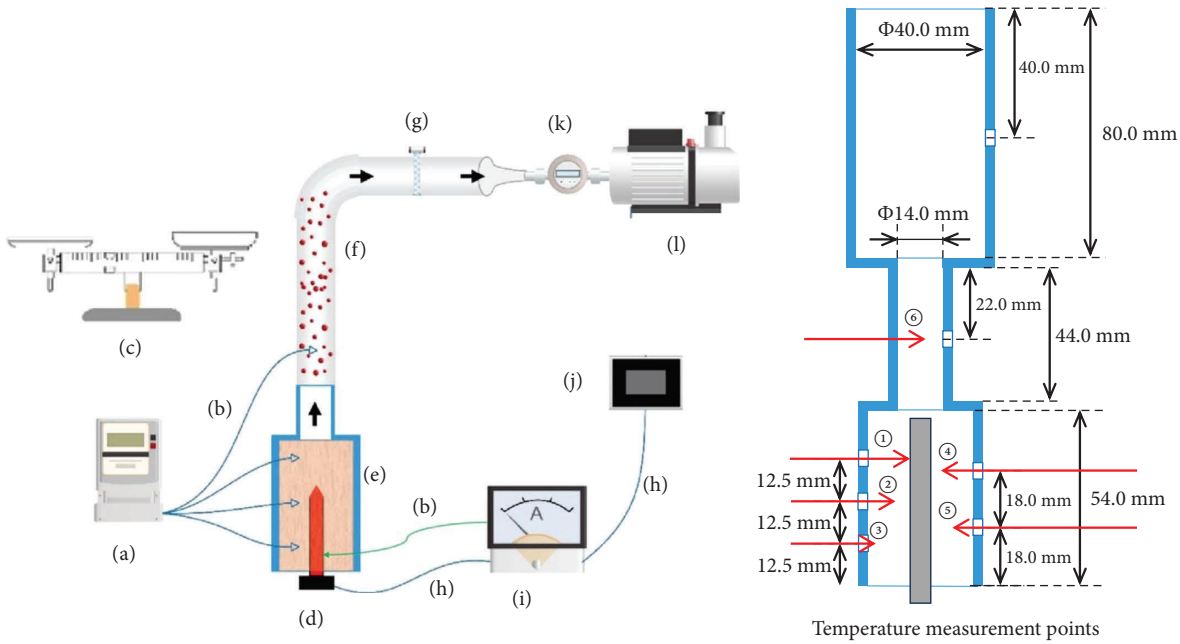

Figure 6: Schematic diagram of the scale-up experimental device: (a) temperature recorder; (b) thermocouple; (c) electronic balance; (d) heater; (e) sleeve; (f) quartz tube; (g) Cambridge filter; (h) wires; (i) thermostat; (j) power supply; (k) glass rotor flow meter; (l) vacuum pump; ① measurement point on the surface of the heater; ② measurement point at a distance of 0.5R from the surface of the heater; ③ measurement point at a distance of R from the surface of the heater (on the inner wall surface of the sleeve); ④ measurement point at a distance of 0.25R from the surface of the heater; ⑤ measurement point at a distance of 0.75R from the surface of the heater; ⑥ measurement point(s) for the temperature of the aerosol. The letter "R" represents the distance between the inner surface of the sleeve and the surface of the heater, which is 15.6 mm.

Table 4: Geometric parameters of the scale-up experimental device and prototype EHTP stick.

Section	Parameter (mm)	Scale-up device	Prototype
Tobacco section	Length	54.00	13.50
	Diameter	31.20	7.80
Heater	Total length	70.00	19.00
	Heater length	50.00	12.00
	Diameter	6.00	2.15
	Insertion depth	50.00	13.80
Hollow section[a]	Length	48.00	12.00
	Diameter	14.00	3.50
Hollow section[b]	Length	80.00	10.00
	Diameter	40.00	5.20
Filter section	Length	—	8.00
	Diameter	—	7.80

Note. (1) "a" denotes the hollow section of 3.50 mm diameter in Figure 1, "b" denotes the hollow section of 5.20 mm diameter in Figure 1. (2) The scale-up experiment is only conducted on the tobacco section of the prototype tobacco product under equivalent criteria conditions (scaled-up by a factor of 4).

tobacco substrate, the aerosol temperature at measurement point ⑥, and the ambient air temperature. The error within the measurement range of the thermocouple is ≤0.05%, and the temperature acquisition frequency is 10 Hz. In addition, the thermostat (i) regulates the surface temperature of the heater by controlling the on-off operation of the circuit based on the deviation between the measured temperature and the target temperature setting value.

The temperature simulation results of the numerical model are validated by comparing them with the measured temperatures at measurement points ①~⑥. Four repetitions of the experiments are conducted at each temperature measurement point, and the maximum standard deviation value is less than 1.0°C. During the experiment, the temperature is recorded for 400 seconds under the heating condition with a constant flow rate of 6.6 L/min. The comparison between the average measured temperatures and the simulation results is presented in Figure 7. It can be observed that the measured temperature decreases significantly in the radial direction across the porous media of tobacco. After 400 seconds, the measured temperature at 0.25R decreases by 48% compared with the surface temperature of the heater. The simulation results demonstrate that the temperature rise pattern within the porous media of the tobacco accumulation body exhibits a good fit with the measured results, with a maximum deviation of less than 15%. The comparative results at 0.25R from the surface of the heater show a relatively greater difference, which may be attributed to the fact that the numerical model is based on the assumption of isotropy in porous media, while the tobacco shreds in the tube furnace are manually filled, leading to potential regions of nonuniform stacking that exhibits anisotropic heat conduction. In addition, the observed fluctuations in experimentally measured temperatures may be attributed to unavoidable fluctuations in the positioning of the thermocouple probe, thereby resulting in slight instability in temperature measurements, while a uniform flow

velocity is specified at the outlet of the numerical model; thus, the simulated temperature curves do not show significant fluctuations.

3.3.2. Validation of the Residual Content in the Tobacco Substrate. The reaction kinetic simulation results are validated by comparing them with the experimental values of the residual contents of water, glycerol, and nicotine in the tobacco substrate. During the experiments, five sets of EHTP sticks each were mounted and fixed onto the corresponding puff channels of the X500E rotary smoking machine. The smoking machine is then set to execute the HCI puffing protocol (55 mL, 2 s sinusoidal puffs every 30 s) for each EHTP stick, with the number of puffs starting from $n = 1$, $n = 2$, ..., and up to $n = 8$. After each puffing protocol ends, the EHTP sticks are immediately removed from the smoking machine and placed together in a 50 mL centrifuge tube. Their mass is weighed and recorded, followed by the addition of the appropriate volume of extraction solvent, and then, the mixture is agitated in preparation for gas chromatographic analysis to determine the residual content of water, glycerol, and nicotine in the tobacco substrate. Three parallel experiments are conducted for each component, and the relative deviation (RD%) between the results is less than 10%, which ensures the reliability and consistency of the obtained data.

Before the first puff starts, the initial amounts of water, glycerol, and nicotine in the tobacco substrate are measured to be 35.98 ± 0.89 mg, 52.09 ± 1.79 mg, and 3.62 ± 0.05 mg, respectively. Accordingly, the initial conditions of the simulation are set to be consistent with the mean values of the abovementioned experimental results. The comparison between the numerical simulation results and the measured values is listed in Table 5. The average prediction errors for the residual amounts of water, glycerol, and nicotine in the tobacco substrate during puffing are 7.13%, 14.90%, and 15.81%, respectively. In general, the model exhibits good predictive performance. The simulation error for nicotine residuals is primarily observed during the 3rd to 5th puffs. This is because the residual amount is tested after a specific number of puffs. Therefore, the results are susceptible to the cumulative effects of experimental and measurement errors. Additionally, the total amount of nicotine in the tobacco substrate is relatively small, which tends to magnify the overall error in the comparison of the experimental and simulated values.

4. Results and Discussion

4.1. The Initial Component Ratio. To investigate the influence of different amounts of water and glycerol on the overall heat transfer effect within the tobacco section and the release characteristics of the three key components, five different initial component ratios are set: (1) 5% water content and 12% glycerol content; (2) 5% water content and 22% glycerol content; (3) 10% water content and 12% glycerol content; (4) 10% water content and 17% glycerol content; and (5) 15% water content and 12% glycerol

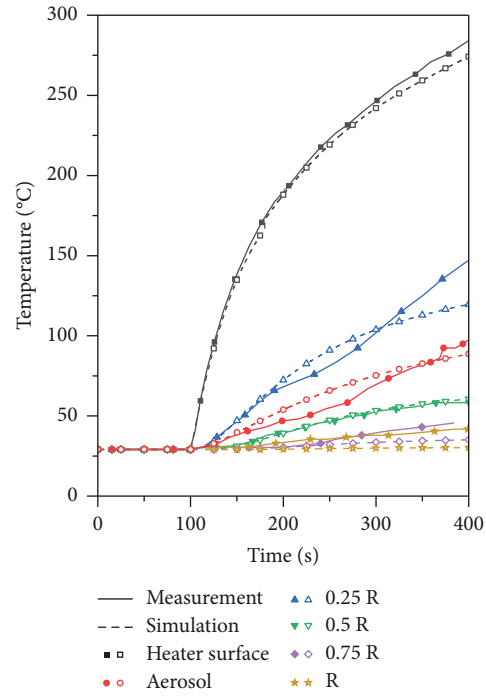

Figure 7: Comparison between the measured temperatures of the scale-up experimental device and the simulation results ("aerosol" refers to the aerosol temperature; 0.25R refers to the internal temperature within the tobacco substrate at a distance of 0.25R from the surface of the heater. The naming principles for the other points are the same).

content. "%" here refers to "weight percent" (wt%). It should be noted that there exists a natural equilibrium correlation between water and glycerol contents in the tobacco substrate of the EHTP, as glycerol acts as a humectant and will equilibrate the water content of the substrate [9]. In this regard, the main objective of this section is focused on conducting a quantitative analysis of the influence of the relative content between water and glycerol. Additionally, as nicotine is a substance naturally contained in tobacco leaves, a consistent nicotine content of 1.13%, which is determined through experimental testing, is set in the simulation.

The puff-by-puff release amount and release efficiency of the three key components corresponding to the five initial component ratio conditions are shown in Figure 8. In all five working conditions, the water release efficiency is approximately 90%. The higher the water content, the lower the release efficiency, and the larger the variance values during individual puffs, which indicates poorer puff-by-puff release uniformity. This is because the water and glycerol contents will affect the thermal conductivity of the tobacco section, thereby affecting the heat transfer process. Figure 9 illustrates the changes in thermal conductivity of the tobacco section with different water and glycerol contents, corresponding to working conditions 2, 4, and 5, respectively, at representative time points ($t = 0$, $t = 50$ s, $t = 100$ s, and $t = 200$ s) during heating. The time points are listed below each image, and the water and glycerol contents are labeled above each column. For working condition 2 (5% water content and 22% glycerol content) with lower water content,

Table 5: Model validation of the residual contents in the tobacco substrate.

Puff number	Water (mg)		Glycerol (mg)		Nicotine (mg)	
	Measurement	Simulation	Measurement	Simulation	Measurement	Simulation
1	27.15 ± 1.04	27.76	50.54 ± 0.25	50.28	3.14 ± 0.04	3.31
2	17.79 ± 0.53	13.51	48.57 ± 0.71	47.13	2.86 ± 0.04	2.85
3	11.22 ± 0.50	9.03	45.31 ± 1.64	46.02	2.76 ± 0.14	2.62
4	7.36 ± 0.05	7.14	45.79 ± 0.45	44.24	2.77 ± 0.09	2.48
5	5.06 ± 0.01	6.00	43.78 ± 0.31	43.12	2.47 ± 0.06	2.36
6	3.61 ± 0.19	5.06	41.15 ± 0.59	41.83	2.42 ± 0.11	2.24
7	2.69 ± 0.07	4.44	39.62 ± 1.08	40.76	2.23 ± 0.03	2.15
8	2.59 ± 0.03	4.00	39.58 ± 0.02	39.86	1.92 ± 0.06	2.08
Mean deviation (%)	7.13		14.90		15.81	

since most of the water has been released in the first 50 s, the influence of water content is less in the later stage of heating. Therefore, the distribution of thermal conductivity is relatively uniform. The stratification of thermal conductivity along the radial direction is obvious under working condition 5 (15% water content and 12% glycerol content) where the water content is similar to the glycerol content. As the water and glycerol components are completely released near the surface of the heater, the thermal conductivity of this area is significantly lower. Meanwhile, the peripheral area of the tobacco section has a lower temperature. As a result, the distribution of thermal conductivity forms a band between the surface of the heater and the periphery.

It can also be seen in Figure 8 that an increase in the initial content of both water and glycerol can significantly enhance their release amounts. At the same glycerol content, a lower water content in the tobacco substrate results in higher glycerol release efficiency. As the water content decreases from 15% to 10%, the glycerol release efficiency increases from 22.93% to 24.37%, but excessively low water content will make the aerosol dry [43]. The impact of different water and glycerol contents on the release of nicotine is more pronounced in the 3rd to 5th puffs, and when the water content is slightly lower than the glycerol content (as in working condition 3 in the simulation), the release efficiency and puff-by-puff release uniformity of nicotine are relatively better.

4.2. The Tobacco Filler Mass. For tobacco substrate with an initial water content of 11.38%, glycerol content of 16.48%, and nicotine content of 1.13%, five groups of tobacco filler mass (220 mg, 280 mg, 320 mg, 360 mg, and 410 mg) are simulated to explore their impacts on heat transfer and the release characteristics of the three key components.

The volume fraction of tobacco in six temperature ranges from room temperature to 350°C is shown in Figure 10. The periodic changes in volume fraction over time can be attributed to changes in the temperature distribution within the tobacco section. Due to the rapid cooling effect of the periodic puffing airflow, the forced convective heat transfer between the incoming airflow and heated tobacco leads to a decrease in the overall average temperature of the tobacco section, which is represented by periodic sharp peaks in the volume fraction within the low-temperature ranges. Besides, it can be observed that the puffing airflow has a more significant impact on tobacco in the temperature ranges of 100~150°C and below 100°C. This is attributed to the higher volume fractions of tobacco in these two temperature ranges. Moreover, tobacco above 250°C tends to accumulate near the surface of the heater, where the airflow velocity is lower. As a result, the volume fraction of tobacco in the high-temperature range is less affected by the puffing airflow.

Comparing the five filler mass conditions, it turns out that with the increase in filler mass, the volume fraction of tobacco in the high-temperature regions gradually increases and the overall average temperature of the tobacco section is relatively higher, with the simulation results of 123.90°C, 127.57°C, 130.82°C, 133.83°C, and 138.31°C, respectively, at the end of the puffing protocol. From the perspective of heat transfer, this is because as the filler mass increases, the porosity of the porous media of tobacco decreases. Although the increase in tobacco filler mass also leads to an overall rise in the specific heat capacity, the impact of porosity on the increase in thermal conductivity is more significant. As a consequence, based on the assumption of porous media with uniform thermal properties in all directions, heat is transferred faster along the radial direction. As the filler mass increases from 220 mg to 410 mg, the volume fraction of tobacco decreases from 32.55% to 5.31% at temperatures below 100°C, increases from 38.10% to 55.92% in the temperature range of 100~150°C, and increases from 25.28% to 34.14% in the temperature range of 150~200°C during the entire puffing protocol, which helps promote the release of the three key components.

The puff-by-puff release amount and release efficiency of the three key components corresponding to the five filler mass conditions are shown in Figure 11. Overall, increasing the tobacco filler mass could enhance the puff-by-puff release amount and release efficiency of water, glycerol, and nicotine. For every 10 mg increase in the tobacco filler mass, the release amounts of water, glycerol, and nicotine increase by 5.99%, 13.43%, and 10.77%, respectively. This is attributed to the increase in the initial content of each component and the rise in the overall temperature within the tobacco section. As the tobacco filler mass increases from 320 mg to 360 mg, the increase in the release amounts of glycerol and nicotine is the most significant. However, the puff-by-puff release uniformity deteriorates with the increase in filler mass. Moreover, excessively high filler mass (410 mg) would

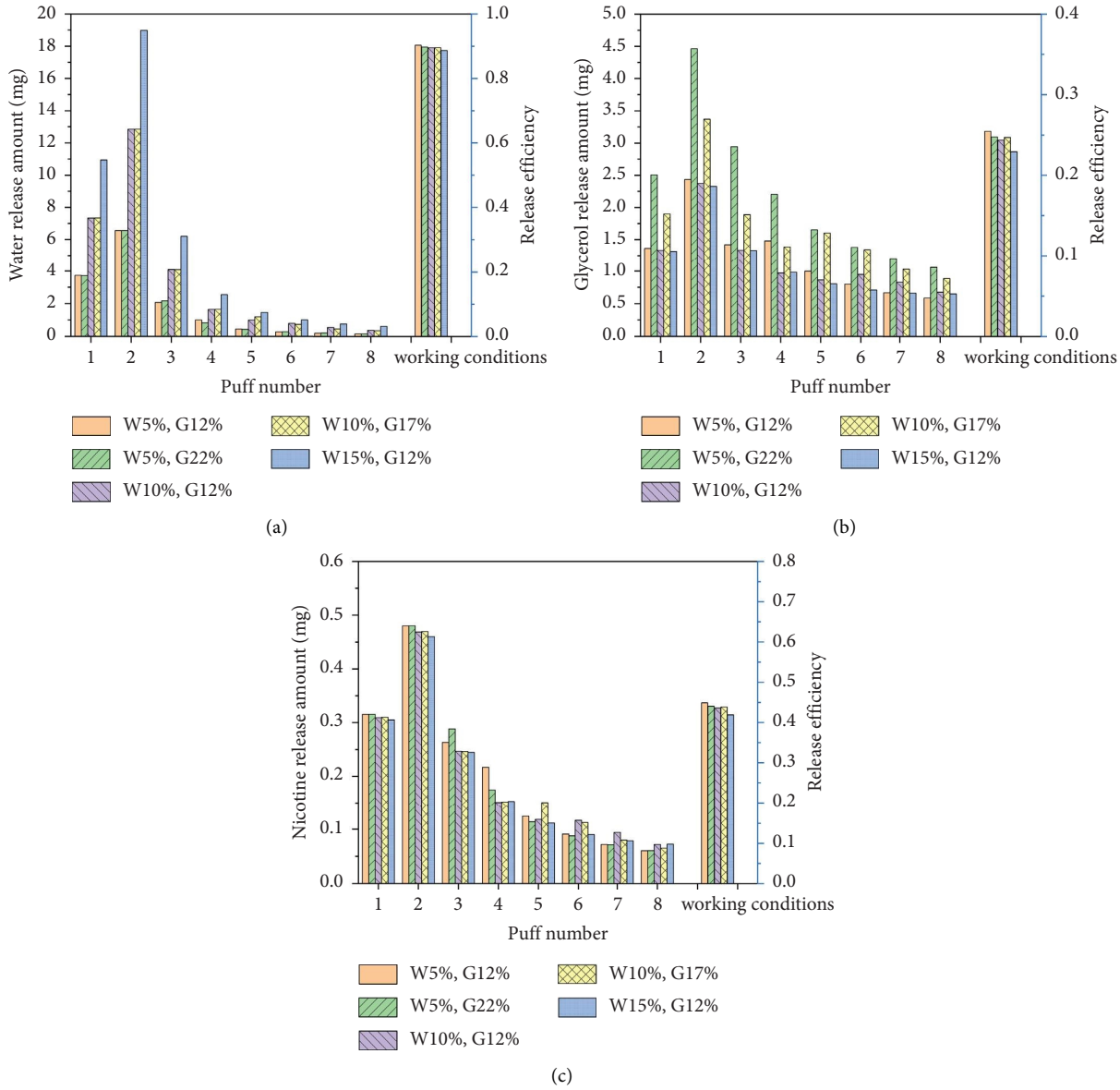

Figure 8: Puff-by-puff release amount and release efficiency of (a) water, (b) glycerol, and (c) nicotine corresponding to different initial component ratio conditions ("W5%, G12%" refers to 5% water content and 12% glycerol content in the tobacco substrate. The naming principles for the other working conditions are the same).

also lead to increased resistance during puffing. Within the range of the studied filler masses (ranging from 220 mg to 410 mg), the maximum resistance during puffing increases from 1853 Pa to 8591 Pa. Therefore, it can be concluded that both excessive and insufficient tobacco filler masses will lead to a less satisfactory aerosol taste.

4.3. The Diameter and Length of the Tobacco Section. To investigate the impact of the diameter and length of the tobacco section on temperature distribution and the release characteristics of the three key components, the diameter and length of the prototype EHTP ($\Phi 7.8 \times 13.5$ mm) are modified ("$\Phi 7.8 \times 13.5$ mm" denotes the dimensions of the EHTP's tobacco section, where "$\Phi 7.8$" represents its diameter and "13.5 mm" represents its length. The naming principles for the other working conditions are the same). Four different tobacco section dimensions ($\Phi 6.8 \times 13.5$ mm, $\Phi 8.8 \times 13.5$ mm, $\Phi 7.8 \times 11.5$ mm, and $\Phi 7.8 \times 15.5$ mm) with the same tobacco filler mass of 320 mg are simulated, respectively.

As the nonequilibrium model of porous media solves the energy equations separately for the gas phase and solid phase, the temperature distribution in both the gas-phase and solid-phase domains can be obtained. The temperature distribution in these two domains at the third puff ($t = 106$ s) is shown in Figure 12. In the radial outward direction from the heater's surface, there is a stratified temperature distribution for both the gas and solid phases in the tobacco section, with temperatures gradually decreasing from the

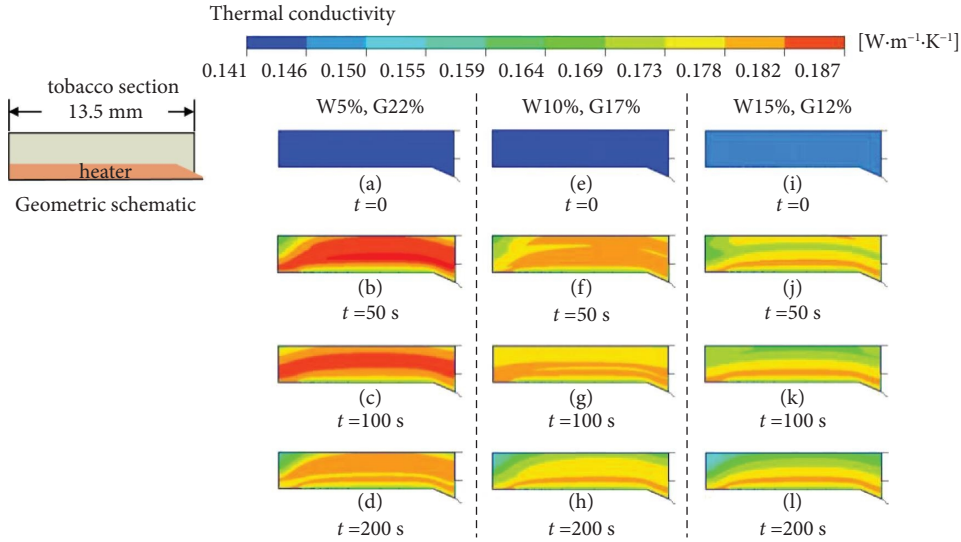

Figure 9: Changes in thermal conductivity of the tobacco section during heating with 5% water content and 22% glycerol content at (a) initial moment, (b) 50 s, (c) 100 s, and (d) 200 s; with 10% water content and 17% glycerol content at (e) initial moment, (f) 50 s, (g) 100 s, and (h) 200 s; with 15% water content and 12% glycerol content at (i) initial moment, (j) 50 s, (k) 100 s, and (l) 200 s.

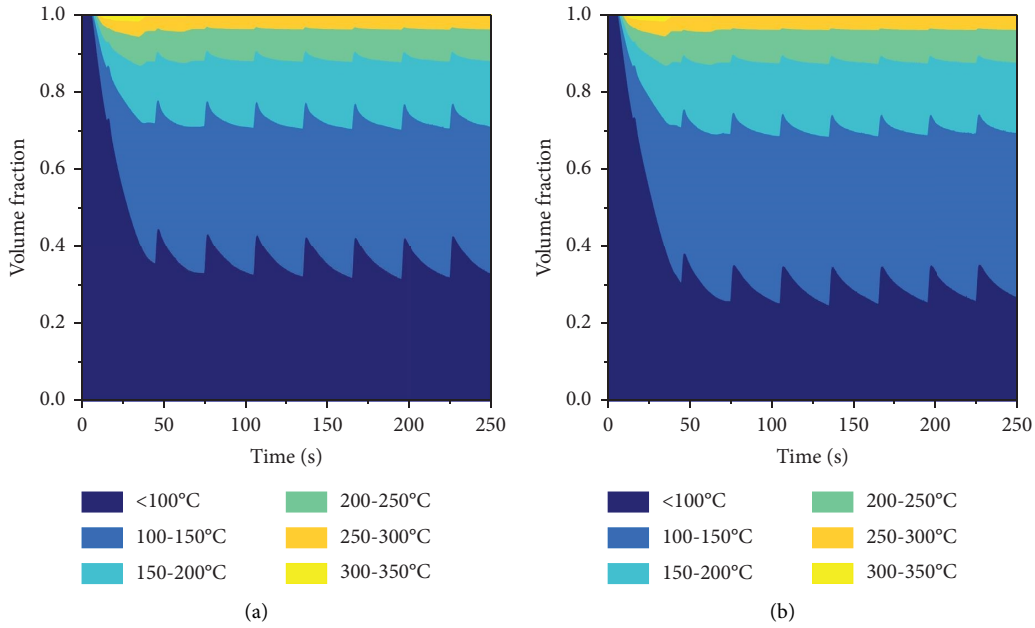

Figure 10: Continued.

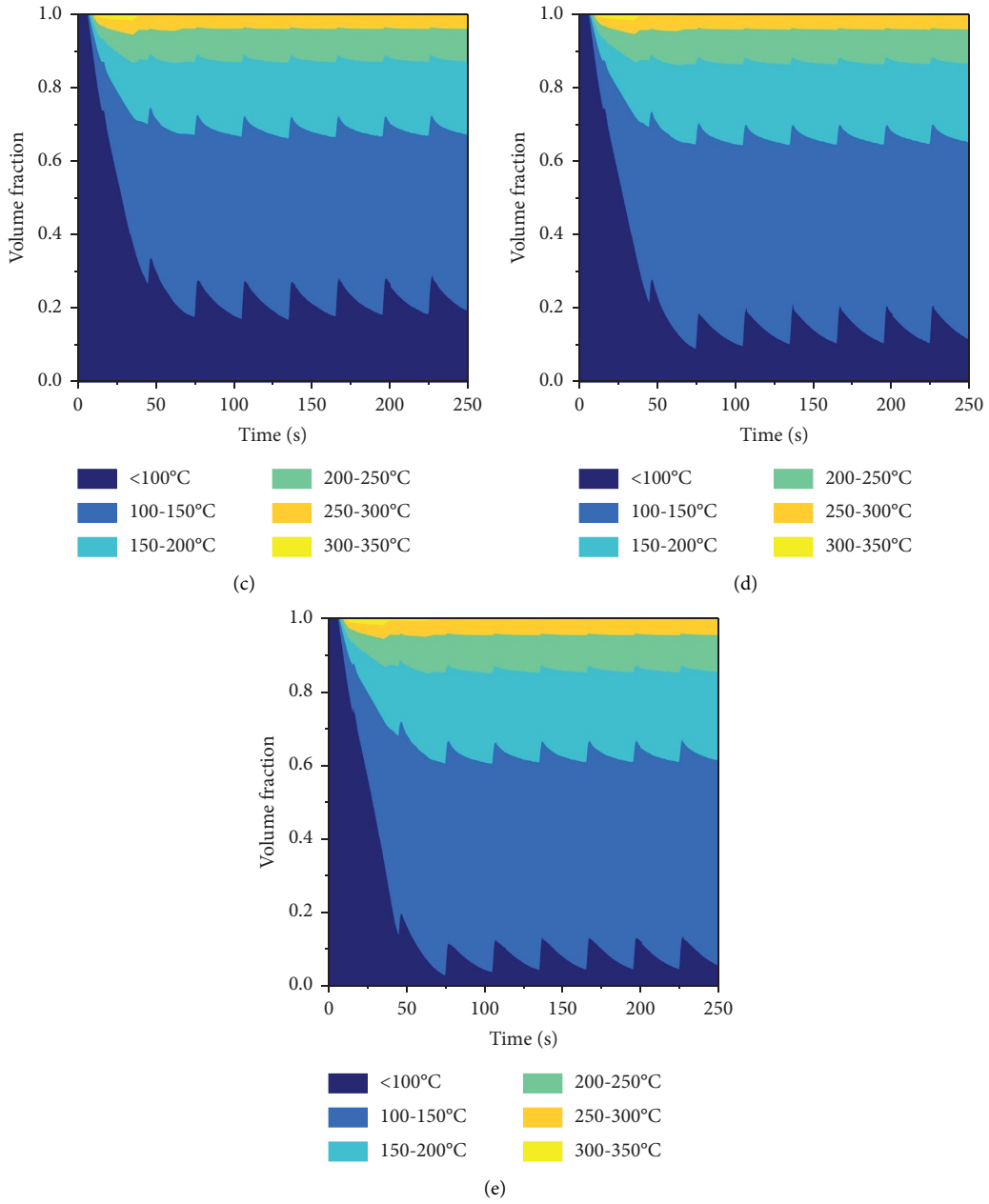

Figure 10: Volume fraction of tobacco in six temperature ranges with the filler mass of (a) 220 mg; (b) 280 mg; (c) 320 mg; (d) 360 mg; (e) 410 mg.

heater's surface toward the periphery. By reducing the diameter of the tobacco section to 6.8 mm, the majority of temperatures within the tobacco substrate are in the range of 100~200°C. According to the volume fraction temperature range statistics, there is an increase in the volume fraction of tobacco from 8.89% to 13.57% within the temperature range of 200°C to 250°C, which is beneficial for the release of the three key components and facilitates the efficient utilization of tobacco. Reducing the length of the tobacco section to 11.5 mm, the low-temperature regions directly above the tip and adjacent to the acetate wall of the hollow section are eliminated. Therefore, it is concluded that reducing the diameter or length of the tobacco section is equivalent to removing tobacco that does not reach the temperature required for the initial release of components. As a result, the overall temperature of the tobacco section increases, and the temperature distribution is more uniform.

However, extending the length of the tobacco section to 15.5 mm will result in insufficient heating of the peripheral tobacco near the tip of the heater and its adjacent area. Once widening the diameter of the tobacco section, the heat transfer range in the radial direction is expanded. The temperature in the widened area is about 68~89°C, which does not reach the peak release temperatures of the three key components. Additionally, extending either the diameter or the length will increase the volume of the tobacco section.

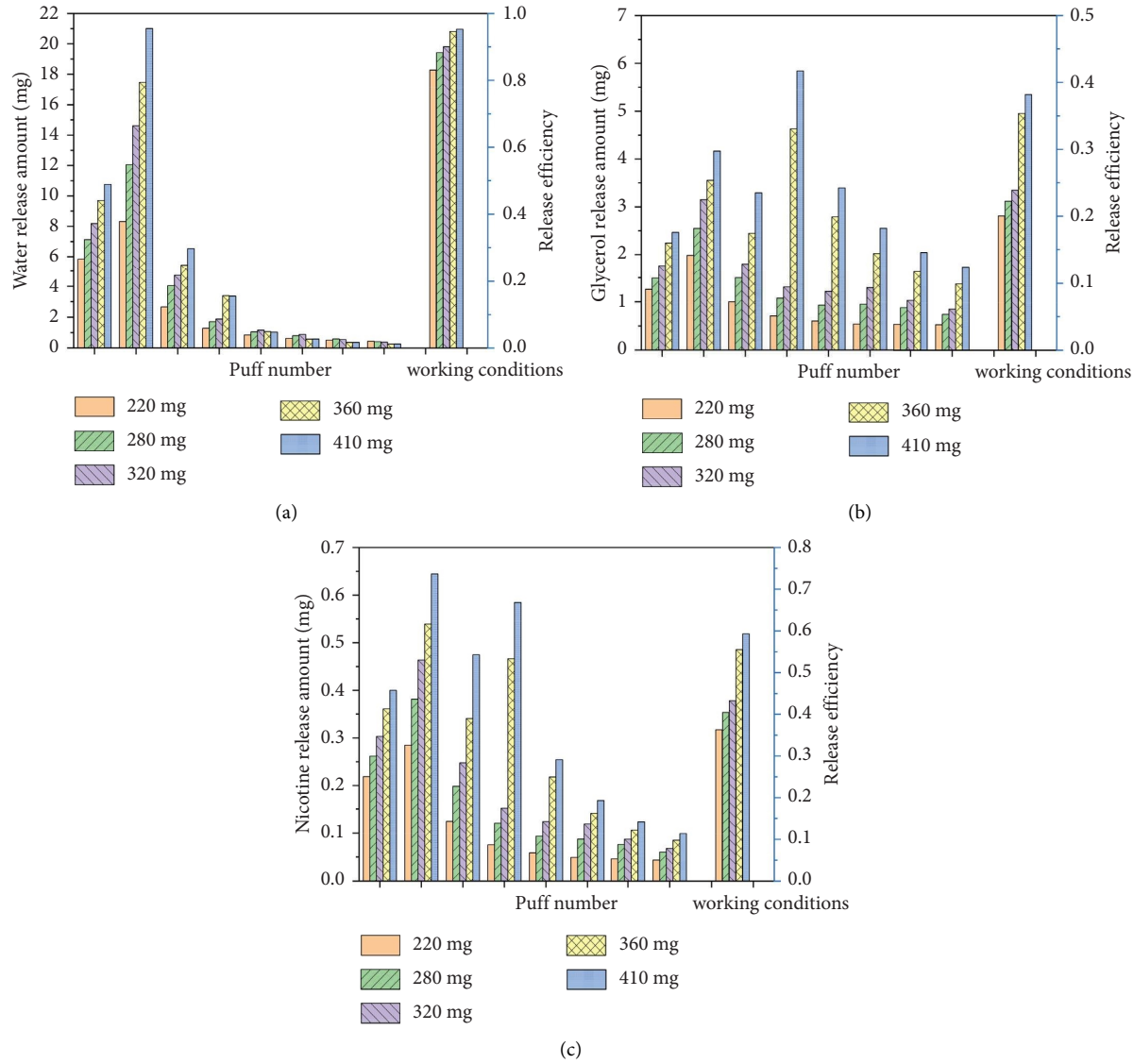

Figure 11: Puff-by-puff release amount and release efficiency of (a) water, (b) glycerol, and (c) nicotine corresponding to different tobacco filler mass conditions ("220 mg" refers to the working condition with a tobacco filler mass of 220 mg. The naming principles for the other working conditions are the same).

Under the same tobacco filler mass condition, it is equivalent to increasing the porosity of the porous media of tobacco, which results in a decrease in the overall thermal conductivity of the tobacco section and hinders the heat transfer process.

The puff-by-puff release amount and release efficiency of the three key components corresponding to different dimensions of the EHTP's tobacco section are shown in Figure 13. Reducing the diameter of the tobacco section to 6.8 mm, a notable increase is observed in the release amounts of components, especially for glycerol and nicotine. Correspondingly, reducing the length of the tobacco section to 11.5 mm increases the release efficiency of water and glycerol by 4.22% and 10.90%, respectively. However, it should be noted that the accelerated heat transfer process in these two working conditions leads to a more pronounced difference in the release amounts between the first three puffs and the last three puffs, which has a negative effect on the puff-by-puff release uniformity. Extending the diameter or length based on the prototype dimension of the EHTP's tobacco section by 2 mm results in a decrease in the component release efficiency, ranging from 7.97% to 29.89%. As previously mentioned, this is attributed to the increase in the volume fraction of tobacco below 100°C, and these low-temperature regions fail to meet the conditions required for the initial release of glycerol and nicotine.

To sum up, with other conditions held constant, extending both the diameter or length of the EHTP's tobacco section will result in a decrease in the release efficiency of components and may lead to underutilization of tobacco materials. Conversely, reducing the diameter or length of the tobacco section could effectively increase the average temperature of the tobacco section and promote component release. However, excessively small dimensions of the

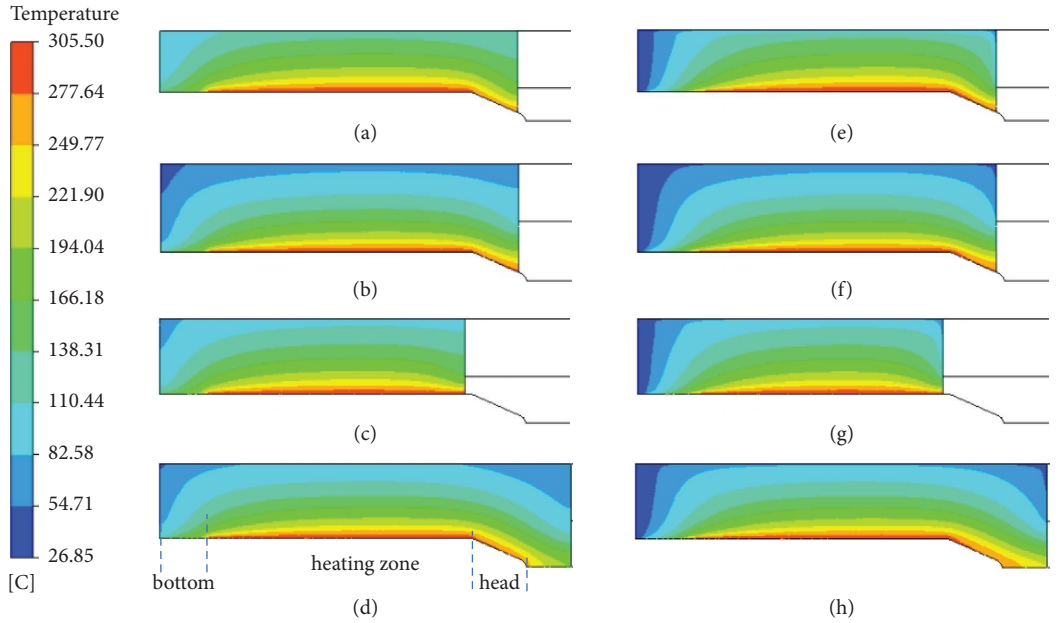

Figure 12: Temperature distribution in the solid-phase domain: (a) Φ6.8 × 13.5 mm; (b) Φ8.8 × 13.5 mm; (c) Φ7.8 × 11.5 mm; (d) Φ6.8 × 15.5 mm; temperature distribution in the gas-phase domain: (e) Φ6.8 × 13.5 mm; (f) Φ8.8 × 13.5 mm; (g) Φ7.8 × 11.5 mm; (h) Φ6.8 × 15.5 mm. $t = 106$ s. The capital letter "Φ" denotes the diameter of the EHTP's tobacco section.

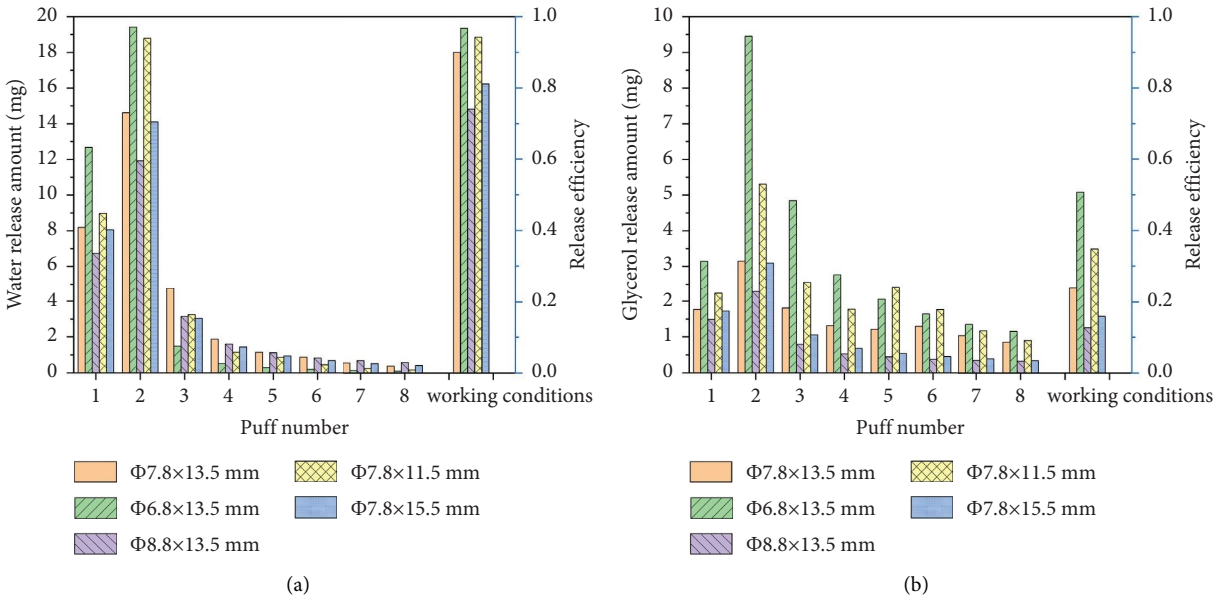

Figure 13: Continued.

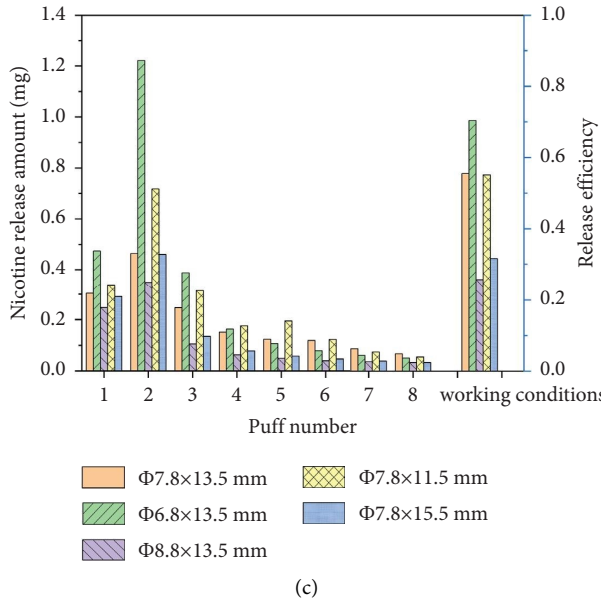

(c)

Figure 13: Puff-by-puff release amount and release efficiency of (a) water, (b) glycerol, and (c) nicotine corresponding to different EHTP dimensions conditions.

tobacco section will result in the nonuniform release of components in each puff, thereby affecting the puffing experience. Moreover, changes in the diameter of the tobacco section have a more pronounced impact than changes in its length, as changes in diameter will result in a more significant change in the volume of the tobacco section.

4.4. The Temperature Profile of the Heater. The design of the temperature profile reflects the heating characteristics of the heater and directly influences the heat transfer process within the tobacco section of the EHTP. To qualitatively explore the influence of the heating mode on the internal heat transfer and the release characteristics of the three key components within the tobacco section, three different time-dependent temperature profiles of the heater are studied and compared. Among them, temperature profile (A) represents the temporal temperature change in the heater in the current EHTP, which is derived from experimentally measured data of the heater's surface temperature. On the basis of temperature profile (A), two additional temperature profiles, (B) and (C), are designed, as shown in Figure 14. Temperature profile (B) exhibits an average temperature and temperature change trend that are essentially consistent with those of temperature profile (A). However, it is specifically designed to facilitate the release of components by canceling the initial 5-second heating phase of the current EHTP, thus initiating heating immediately upon product activation. Additionally, a stepped temperature rise is introduced after 170 seconds to further increase the temperature of the tobacco section and explore its potential effect on promoting the release of components during the last few puffs. The temperature profile (C) is designed to investigate the impact of heating rate on component release by employing a continuous progressive heating mode. In this mode, the surface temperature of the heater gradually rises to 304.95°C during 150 seconds and then remains constant. With the above three temperature profiles, simulations are conducted for the EHTP with a tobacco section dimension of $\Phi 7.8 \times 13.5$ mm and the tobacco filler mass of 320 mg.

The puff-by-puff release amount and release efficiency of the three key components corresponding to the three temperature profiles are shown in Figure 15. The results indicate that by adopting the temperature profile (B), the release amounts of the three components in the first two puffs increase significantly, as well as the release efficiency. The increase in glycerol release is the most obvious, with an increase in the amount ranging from 0.06 to 2.39 mg per puff in comparison with the working condition adopting the temperature profile (A). However, it also leads to a lower residual component content in the last three puffs, and the designed "stepped temperature rise" is insufficient to compensate for the reduced release amounts of components. As a result, there is a significant difference in the total release amounts between the early and late stages of puffs. The heating temperature of profile (C) rises slowly in the first 70 seconds; therefore, the release process of components is the slowest, as it is directly associated with the rate of heat transfer. It can be observed that water is predominantly released between the 2nd and 4th puffs, while the release peak of glycerol occurs at the 6th puff, which contributes to regulating the uniformity of component content in the aerosol to some extent. Compared with the temperature profile (A), the release efficiency of water, glycerol, and nicotine in this case is slightly increased by 1.35%, 2.60%, and 2.63%, respectively.

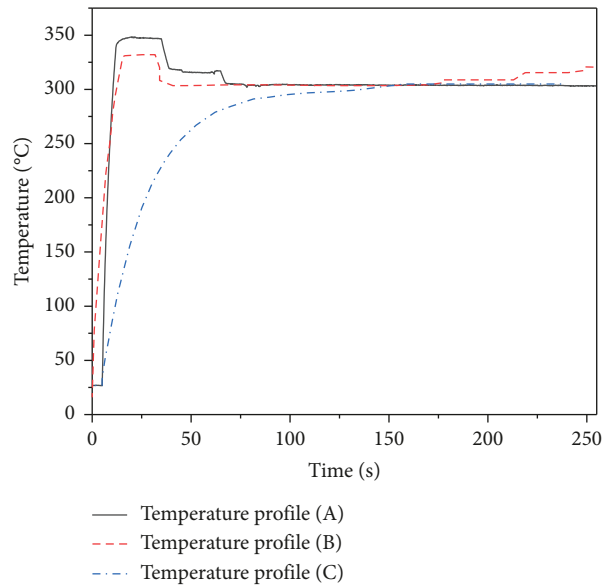

Figure 14: Three kinds of temperature rise curves on the heater surface.

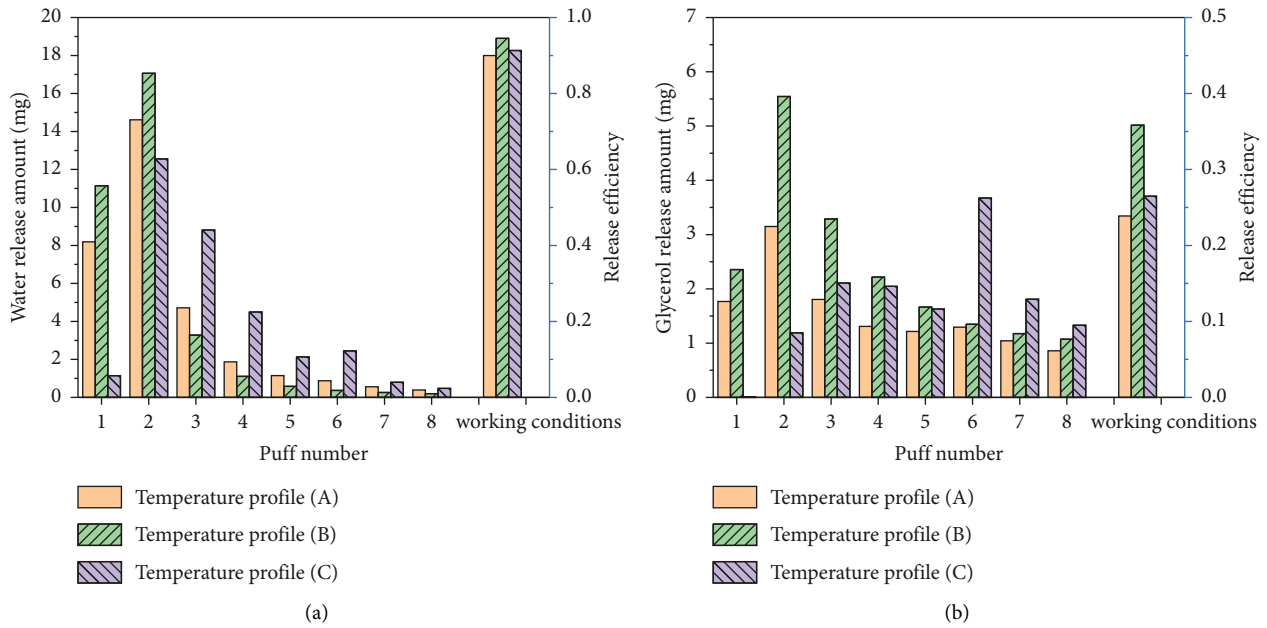

Figure 15: Continued.

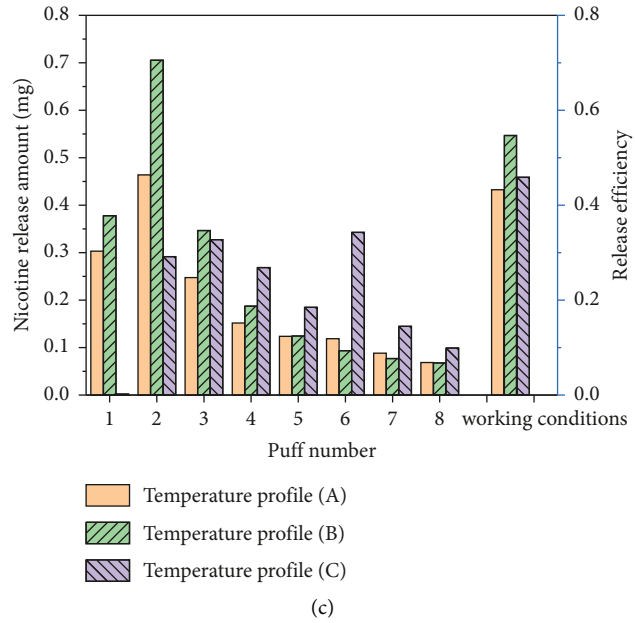

Figure 15: Puff-by-puff release amount and release efficiency of (a) water, (b) glycerol, and (c) nicotine corresponding to different temperature profiles of the heater ("temperature profile (A)" refers to the working condition adopting the temperature profile (A). The naming principles for the other working conditions are the same).

Table 6: Experimental results of the thermal properties of tobacco sheets at different temperatures.

Water content (%)	Glycerol content (%)	Temperature (°C)	Thermal conductivity ($W \cdot m^{-1} \cdot K^{-1}$)	Volumetric heat capacity ($MJ \cdot m^{-3} \cdot K^{-1}$)
9.08 ± 0.05	0.00 ± 0.00	20 ± 0.2	0.2045 ± 0.0017	1.5729 ± 0.0090
		100 ± 0.5	0.3614 ± 0.0025	2.4639 ± 0.0157
		200 ± 1.0	0.3075 ± 0.0014	1.9346 ± 0.0141
		300 ± 0.6	0.2106 ± 0.0015	1.9300 ± 0.0219
9.63 ± 0.07	9.67 ± 0.05	20 ± 0.2	0.2008 ± 0.0013	1.4570 ± 0.0082
		100 ± 0.5	0.3585 ± 0.0022	2.4320 ± 0.0192
		200 ± 1.0	0.2968 ± 0.0019	2.2860 ± 0.0115
		300 ± 0.6	0.2032 ± 0.0009	1.7450 ± 0.0121
9.39 ± 0.09	19.64 ± 0.10	20 ± 0.2	0.2560 ± 0.0016	2.0180 ± 0.0198
		100 ± 0.5	0.3674 ± 0.0020	3.0660 ± 0.0219
		200 ± 1.0	0.2834 ± 0.0021	2.5070 ± 0.0164
		300 ± 0.6	0.1708 ± 0.0008	1.7380 ± 0.0149
7.90 ± 0.11	31.53 ± 0.15	20 ± 0.2	0.2770 ± 0.0011	2.1160 ± 0.0153
		100 ± 0.5	0.3430 ± 0.0018	3.1670 ± 0.0265
		200 ± 1.0	0.2870 ± 0.0013	2.6440 ± 0.0099
		300 ± 0.6	0.1690 ± 0.0010	1.5260 ± 0.0138
14.47 ± 0.06	30.25 ± 0.10	20 ± 0.2	0.3070 ± 0.0012	2.4770 ± 0.0176
		100 ± 0.5	0.3680 ± 0.0020	3.2710 ± 0.0254
		200 ± 1.0	0.2750 ± 0.0025	2.7290 ± 0.0158
		300 ± 0.6	0.1750 ± 0.0012	1.2240 ± 0.0128

Table 7: Parameter fitting results of the thermal conductivity model.

Temperature range (°C)	a	b	c	k_{b0}	d
20~100	1.4240	−0.9530	−0.4412	0.0332	0.0994
>100				0.5013	−0.0020

Table 8: Experimental results of the thermal properties of tobacco accumulation body.

Water content (%)	Glycerol content (%)	Temperature (°C)	Filler density ($kg \cdot m^{-3}$)	Thermal conductivity ($W \cdot m^{-1} \cdot K^{-1}$)
10.62 ± 0.06	19.00 ± 0.14	22 ± 0.2	360 ± 2	0.0930 ± 0.0006
			420 ± 2	0.1028 ± 0.0005
			480 ± 2	0.1127 ± 0.0004
			600 ± 2	0.1361 ± 0.0009
5.53 ± 0.14	19.00 ± 0.12	24 ± 0.2	480 ± 2	0.0961 ± 0.0009
10.10 ± 0.04				0.1115 ± 0.0015
12.87 ± 0.08				0.1344 ± 0.0007
16.67 ± 0.11				0.1416 ± 0.0018

Table 9: Thermal conductivity calculated by the thermal conductivity model and its deviation from the experimental values.

Water content (%)	Glycerol content (%)	Temperature (°C)	Porosity	V_w	V_{gly}	Thermal conductivity ($W \cdot m^{-1} \cdot K^{-1}$)	Deviation (%)
10.62	19.00	22	0.6538	0.1338	0.1898	0.0882	5.12
			0.5961			0.1010	1.72
			0.5385			0.1135	0.68
			0.4231			0.1380	1.35
5.53	19.00	24	0.5385	0.0708	0.1928	0.1090	13.40
10.10				0.1275	0.1901	0.1139	2.17
12.87				0.1611	0.1886	0.1164	13.43
16.67				0.2063	0.1865	0.1192	15.86

5. Conclusions

In this study, a coupled mathematical model of gas flow, heat transfer, and the release of key components in an electrically heated tobacco product is established. The release rates of water, glycerol, and nicotine are quantitatively described by the first-order Arrhenius function. The influences of several important parameters, including the initial component ratio, the tobacco filler mass, the diameter and length of the EHTP's tobacco section, and the temperature profile of the heater, are studied using CFD simulation. The major conclusions are listed as follows:

(1) Increasing the initial water and glycerol content in the tobacco substrate can increase the total release amounts, but the higher the water content, the lower the release efficiency of the key components and the poorer the puff-by-puff release uniformity.

(2) Increasing the mass of the tobacco filler can increase the thermal conductivity and average temperature of the tobacco section. For every 10 mg increase in the tobacco filler mass, the release amounts of water, glycerol, and nicotine increase by 5.99%, 13.43%, and 10.77%, respectively.

(3) Based on the prototype EHTP with a tobacco section dimension of $\Phi 7.8 \times 13.5$ mm, a reduction in either the diameter or length of the tobacco section could help increase its overall average temperature, which, in turn, would promote the release of key components. However, it would also have a negative effect on the puff-by-puff release uniformity. Extending the length or diameter of the tobacco section will hinder the heat transfer process and lead to a decrease in the component release efficiency.

(4) A slower heating rate matched with longer preheating times enables the complementary release of water and glycerol components, which helps regulate the uniformity of component content in the aerosol to some extent.

Appendix

According to Krupiczka et al. [44], the approximate solution of the thermal conductivity model of the stacked porous media is as follows:

$$k_e = k_g\left(k_s/k_g\right)^{a-b\log(1-\phi)+c\log\left(k_s/k_g\right)}, \quad (A.1)$$

where k_e is the effective thermal conductivity, W/(m·K); k_g is the thermal conductivity of gas, W/(m·K); k_s is the thermal conductivity of wet tobacco material, W/(m·K); and ϕ is the porosity of the tobacco accumulation body. The values of a, b, and c are constants and can be obtained by fitting the experimental data.

The thermal property of wet tobacco material is mainly affected by the inner skeleton of tobacco and water and glycerol contents in the pores. Assuming that the two liquid components and tobacco particles are randomly distributed, the spatial random distribution model of Tavman et al. [45] can be used to calculate the thermal conductivity of the tobacco substrate:

$$k_s = k_w^{V_w} k_{gly}^{V_{gly}} k_b^{\left(1-V_w-V_{gly}\right)}, \quad (A.2)$$

where k_w is the thermal conductivity of liquid water, W/(m·K); V_w is the volume fraction of liquid water in tobacco particles; k_{gly} is the thermal conductivity of liquid glycerol, W/(m·K); k_b is the thermal conductivity of the solid skeleton, and for homogeneous solids, it can be considered to have a linear relationship with temperature, $k_b = k_{b0}(1 + dT)$, W/(m·K); k_{b0} is the thermal conductivity of solid particles at 0°C under atmospheric pressure, W/(m·K); and d is a constant.

The Hot Disk TPS 2500 S instrument is used to test the thermal properties, including the thermal conductivity and volumetric heat capacity of the tobacco sheets with five different components at 20~300°C. Air atmosphere is used at room temperature, and helium atmosphere is used at high temperature. Three parallel experiments are conducted for each working condition. The experimental results are presented in Table 6. Based on the measured values, by fitting the functions of equations (1) and (2), the results of each coefficient are obtained in Table 7.

Furthermore, the thermal properties of the tobacco accumulation body with four different filler densities and five different water contents are measured at room temperature. Three parallel experiments are conducted for each working condition. The experimental results are presented in Table 8.

Within the investigated range of temperature and water content, the comparison of the thermal conductivity predicted by the thermal conductivity model with the experimental values is presented in Table 9, with an average deviation of 6.72% and a maximum deviation of 15.86%. Therefore, the thermal conductivity model exhibits excellent predictive accuracy over the range of temperatures investigated in this study.

Nomenclature

A_{gs}: Interfacial area density (m^{-1})
A_i: Pre-exponential factor in the Arrhenius formula (s^{-1})
B_f: Body force ($N \cdot m^{-3}$)
C_2: Inertial resistance factor
D_i: Diffusion coefficient of gas-phase component i ($m^2 \cdot s^{-1}$)
E_g: Gas-phase energy ($J \cdot kg^{-1}$)
E_i: Chemical reaction activation energy ($kJ \cdot mol^{-1}$)
E_s: Solid-phase energy ($J \cdot kg^{-1}$)
g: Gas phase
h: Enthalpy ($J \cdot kg^{-1}$)
h_{gs}: Heat transfer coefficient for the fluid/solid interface ($W \cdot m^{-2} \cdot K^{-1}$)
h_i: Enthalpy of gas-phase component i ($J \cdot kg^{-1}$)
ΔH_k: Energy absorbed per unit mass of component k during phase transition ($J \cdot kg^{-1}$)
i: A specific component in the gas phase
J_i: Diffusion flux of gas-phase component i ($kg \cdot m^{-3} \cdot s^{-1}$)
k: A specific component in the solid phase
k_g: Gas-phase thermal conductivity ($W \cdot m^{-1} \cdot K^{-1}$)
k_i: Chemical reaction rate (s^{-1})
k_s: Solid-phase thermal conductivity ($W \cdot m^{-1} \cdot K^{-1}$)
m_s: Tobacco filler mass (kg)
n: Number of components
p: Pressure (Pa)
R: Universal gas constant ($J \cdot mol^{-1} \cdot K^{-1}$)
s: Solid phase
S_g^h: Gas-phase enthalpy source term
S_s^h: Solid-phase enthalpy source term
S_i: Source term of porous media
$S_{Y_i}^*$: The maximum mass of component i that can be released under infinite time and high pyrolysis intensity ($mg \cdot mg^{-1}$)
$S_{Y_i}^{s \longrightarrow g}$: Mass of component i released per unit mass of tobacco at each moment ($mg \cdot mg^{-1}$)
$S_\rho^{s \longrightarrow g}$: Mass transfer source term of gas-solid phase per unit volume
$S_{\rho_i}^{s \longrightarrow g}$: Mass transfer source term of component i per unit volume
t: Time (s)
T_g: Gas-phase temperature (K)
T_s: Solid-phase temperature (K)
V: Volume of the entire domain of the tobacco section (m^3)
Y_i: Mass fraction of component i in the gas phase
v: Gas-phase velocity ($m \cdot s^{-1}$)
α: Permeability of porous media (m^2)
ϕ: Porosity of porous media
τ: Stress tensor (Pa)
μ: Dynamic viscosity of the gas phase ($kg \cdot m^{-1} \cdot s^{-1}$)
ρ: Density ($kg \cdot m^{-3}$)
ρ_g: Gas-phase density ($kg \cdot m^{-3}$)
ρ_i: Density of component i in the gas phase ($kg \cdot m^{-3}$)
ρ_k: Density of component k in the solid phase ($kg \cdot m^{-3}$)
ρ_s: Solid-phase density ($kg \cdot m^{-3}$).

Data Availability

The data that support the findings of this study are available from the corresponding authors upon reasonable request.

Conflicts of Interest

The authors declare that they have no conflicts of interest.

Authors' Contributions

B. Zhang and L.J. Xiao contributed equally to this work.

References

[1] U.S. Food and Drug Administration, "Premarket tobacco product marketing orders TPL pm0000424-79," https://www.fda.gov/media/124247/download.

[2] M. I. Mitova, P. B. Campelos, C. G. Goujon-Ginglinger et al., "Comparison of the impact of the Tobacco Heating System 2.2 and a cigarette on indoor air quality," *Regulatory Toxicology and Pharmacology*, vol. 80, pp. 91–101, 2016.

[3] J. Elias and P. M. Ling, "Invisible smoke: third-party endorsement and the resurrection of heat-not-burn tobacco products," *Tobacco Control*, vol. 27, no. Suppl 1, pp. s96–s101, 2018.

[4] H. Gasparyan, D. Mariner, C. Wright et al., "Accurate measurement of main aerosol constituents from heated tobacco products (HTPs): implications for a fundamentally different aerosol," *Regulatory Toxicology and Pharmacology*, vol. 99, pp. 131–141, 2018.

[5] K. Bekki, Y. Inaba, S. Uchiyama, and N. Kunugita, "Comparison of chemicals in mainstream smoke in heat-not-burn tobacco and combustion cigarettes," *Journal of UOEH*, vol. 39, no. 3, pp. 201–207, 2017.

[6] E. Simonavicius, A. McNeill, L. Shahab, and L. S. Brose, "Heat-not-burn tobacco products: a systematic literature review," *Tobacco Control*, vol. 28, no. 5, pp. 582–594, 2019.

[7] M. Nordlund, M. Smith, S. Maeder et al., *Scientific Substantiation of the Absence of Combustion and No Smoke Formation in the Electrically Heated Tobacco Product (EHTP)*, Philip Morris Products SA, Neuchâtel, Switzerland, 2019.

[8] M. S. Werley, S. A. Freelin, S. E. Wrenn et al., "Smoke chemistry, in vitro and in vivo toxicology evaluations of the electrically heated cigarette smoking system series K," *Regulatory Toxicology and Pharmacology*, vol. 52, no. 2, pp. 122–139, 2008.

[9] Y. Gao, J. Huang, J. Gao, J. Wu, Y. Xie, and N. Gao, "Research progress on mechanism behind heat and mass transfer and key substance release of electrically heated tobacco products," *Tobacco Science & Technology*, vol. 55, no. 8, pp. 100–112, 2022.

[10] J. I. Seeman, J. A. Fournier, J. B. Paine, and B. E. Waymack, "The form of nicotine in tobacco. Thermal transfer of nicotine and nicotine acid salts to nicotine in the gas phase," *Journal of Agricultural and Food Chemistry*, vol. 47, no. 12, pp. 5133–5145, 1999.

[11] J. P. Schaller, D. Keller, L. Poget et al., "Evaluation of the Tobacco Heating System 2.2. Part 2: chemical composition, genotoxicity, cytotoxicity, and physical properties of the aerosol," *Regulatory Toxicology and Pharmacology*, vol. 81, pp. S27–S47, 2016.

[12] M. C. Bentley, M. Almstetter, D. Arndt et al., "Comprehensive chemical characterization of the aerosol generated by a heated tobacco product by untargeted screening," *Analytical and Bioanalytical Chemistry*, vol. 412, no. 11, pp. 2675–2685, 2020.

[13] V. Cozzani, F. Barontini, T. McGrath et al., "An experimental investigation into the operation of an electrically heated tobacco system," *Thermochimica Acta*, vol. 684, Article ID 178475, 2020.

[14] T. B. Reed, *Encyclopedia of Biomass thermal Conversion: The Principles and Technology of Pyrolysis, Gasification & Combustion*, Biomass energy foundation Press, Franktown, 2002.

[15] X. Zheng, Z. Li, C. Wang et al., "Study on release characteristics of electrically heat-not-burn cigarette smoke under different heating temperatures," *Journal of Anhui Agricultural Sciences*, vol. 46, no. 36, pp. 168–171, 2018.

[16] A. Gómez-Siurana, A. Marcilla, M. Beltrán, D. Berenguer, I. Martínez-Castellanos, and S. Menargues, "TGA/FTIR study of tobacco and glycerol-tobacco mixtures," *Thermochimica Acta*, vol. 573, pp. 146–157, 2013.

[17] D. Eaton, B. Jakaj, M. Forster et al., "Assessment of tobacco heating product THP1.0. Part 2: product design, operation and thermophysical characterisation," *Regulatory Toxicology and Pharmacology*, vol. 93, pp. 4–13, 2018.

[18] W. Zhu, H. Lin, Y. Cao, and B. Li, "Thermal properties measurement of cut tobacco based on TPS method and thermal conductivity model," *Journal of Thermal Analysis and Calorimetry*, vol. 116, no. 3, pp. 1117–1123, 2014.

[19] Y. Ma, C. Liu, L. Wang et al., "Influences of tobacco's shape on its thermophysical properties," *Tobacco Science & Technology*, vol. 51, no. 6, pp. 90–94, 2018.

[20] F. Barontini, A. Tugnoli, V. Cozzani, J. Tetteh, M. Jarriault, and I. Zinovik, "Volatile products formed in the thermal decomposition of a tobacco substrate," *Industrial & Engineering Chemistry Research*, vol. 52, no. 42, pp. 14984–14997, 2013.

[21] G. Guo, C. Liu, Y. Wang et al., "Comparative investigation on thermal degradation of flue-cured tobacco with different particle sizes by a macro-thermogravimetric analyzer and their apparent kinetics based on distributed activation energy model," *Journal of Thermal Analysis and Calorimetry*, vol. 138, no. 5, pp. 3375–3388, 2019.

[22] J. L. F. Alves, J. C. G. da Silva, G. D. Mumbach et al., "Thermokinetic investigation of the multi-step pyrolysis of smoked cigarette butts towards its energy recovery potential," *Biomass Conversion and Biorefinery*, vol. 12, no. 3, pp. 741–755, 2020.

[23] Y. Mu, Y. Peng, X. Tang et al., "Experimental and kinetic studies on tobacco pyrolysis under a wide range of heating rates," *ACS Omega*, vol. 7, no. 1, pp. 1420–1427, 2021.

[24] F. Meng, H. Cui, M. Fan et al., "Spatially resolved aerosol characterization during thermal distillation and pyrolysis of tobacco using an in-situ microprobe sampling coupled with fast particulate spectrometer," *Journal of Analytical and Applied Pyrolysis*, vol. 170, Article ID 105911, 2023.

[25] D. Tang, J. Wu, J. Zeng, W. Gao, and L. Du, "Research on cigarette during smoking based on reverse engineering and numerical simulation," *Chinese Journal of Chemical Engineering*, vol. 27, no. 10, pp. 2359–2375, 2019.

[26] Z. Sun, W. Wang, W. Du et al., "Electro-thermal simulation of heating element for electrically heated tobacco products," *Tobacco Science & Technology*, vol. 53, no. 9, pp. 85–93, 2020.

[27] Z. Jiang, X. Ding, T. Fang, H. Huang, W. Zhou, and Q. Sun, "Study on heat transfer process of a heat not burn tobacco product flow field," *Journal of Physics: Conference Series*, vol. 1064, no. 1, Article ID 012011, 2018.

[28] W. Xiao, G. Zhou, J. Jiang, A. Hu, W. Zhan, and Y. Guo, "Numerical simulation of heat transfer and smoke flow of heated cigarette product," *Journal of East China University of Science and Technology*, vol. 47, no. 1, pp. 35–40, 2021.

[29] Q. Gui, *CFD Simulation and Experimental Verification of an Electrically Heated Cigarettes Product*, Hunan University, Hu Nan Sheng, China, 2022.

[30] M. Nordlund and A. K. Kuczaj, "Modeling flow, heat and mass transfer in a porous biomass plug—when used in an electrically heated tobacco system," *ECI Symposium Series*, pp. 1–6, 2016.

[31] L. Wang, Y. Wang, Z. Li et al., "Temperature distribution in tobacco section of an electrically heated cigarette and puff-by-puff releases of key smoke components: Part 2 Simulation," *Tobacco Science & Technology*, vol. 54, no. 6, pp. 58–64, 2021.

[32] "Fluent user's guide," 2021, https://ansyshelp.ansys.com/account/secured?returnurl=/Views/Secured/corp/v211/en/flu_ug/flu_ug.html.

[33] H. A. McGee, *Molecular Engineering*, McGraw-Hill, New York, 1991.

[34] A. Rostami, J. Murthy, and M. Hajaligol, "Modeling of a smoldering cigarette," *Journal of Analytical and Applied Pyrolysis*, vol. 66, no. 1-2, pp. 281–301, 2003.

[35] M. S. Saidi, M. R. Hajaligol, and F. Rasouli, "Numerical simulation of a burning cigarette during puffing," *Journal of*

Analytical and Applied Pyrolysis, vol. 72, no. 1, pp. 141–152, 2004.

[36] X. Zhang and T. Zhu, *Q, an. Heat Transfer*, China Architecture & Building Press, Beijing, China, 6th edition, 2014.

[37] G. Liu, L. Ma, and S. Xiang, *Data Handbook of Chemistry and Chemical Engineering — Organic*, Chemical Industry Press, Beijing, 2012.

[38] "CAMEO Chemicals database. [EB/OL]," 2015, http://cameochemicals.noaa.gov/.

[39] J. O. Hirschfelder, C. F. Curtiss, and R. B. Bird, *Molecular Theory of Gases and Liquids*, John Wiley & Sons, New York, 1954.

[40] Cooperation Centre for Scientific Research Relative to Tobacco, "Recommended Methods No. 57, Determination of water in tobacco and tobacco products by gas chromatographic analysis," 2018, https://www.coresta.org/sites/default/files/technical_documents/main/CRM_57-Aug2018.pdf.

[41] Cooperation Centre for Scientific Research Relative to Tobacco, "Recommended Methods No. 60, Determination of 1, 2-propylene glycol and glycerol in tobacco and tobacco products by gas chromatography," 2018, https://www.coresta.org/sites/default/files/technical_documents/main/CRM_60-June2019.pdf.

[42] Cooperation Centre for Scientific Research Relative to Tobacco, "Recommended Methods No. 62, Determination of nicotine in tobacco and tobacco products by gas chromatographic analysis," 2018, https://www.coresta.org/sites/default/files/technical_documents/main/CRM_62-December2021.pdf.

[43] S. Chen, G. Shen, and Y. He, "Filter additive capable of increasing moisture content in cigarette smoke," *Tobacco Science & Technology*, vol. 2014, no. 07, pp. 10–12, 2014.

[44] R. Krupiczka, "Analysis of thermal conductivity in granular materials," *International Chemical Engineering*, vol. 7, no. 1, pp. 122–143, 1967.

[45] I. H. Tavman, "Effective thermal conductivity of granular porous materials," *International Communications in Heat and Mass Transfer*, vol. 23, no. 2, pp. 169–176, 1996.